POMK regulates dystroglycan function via LARGE-mediated elongation of matriglycan

Ameya S. Walimbe[1], Hidehiko Okuma[1], Soumya Joseph[1], Tiandi Yang[1], Takahiro Yonekawa[1], Jeffrey M. Hord[1], David Venzke[1], Mary E. Anderson[1], Silvia Torelli[2], Adnan Manzur[2], Megan Devereaux[1], Marco Cuellar[1], Sally Prouty[1], Saul Ocampo Landa[1], Liping Yu[3], Junyu Xiao[5], Jack E. Dixon[6], Francesco Muntoni[2, 4], and Kevin P. Campbell[1*]

[1]Howard Hughes Medical Institute, Senator Paul D. Wellstone Muscular Dystrophy Specialized Research Center, Department of Molecular Physiology and Biophysics and Department of Neurology, Roy J. and Lucille A. Carver College of Medicine, The University of Iowa, Iowa City, Iowa 52242, USA

[2]Dubowitz Neuromuscular Centre, UCL Great Ormond Street Institute of Child Health & Great Ormond Street Hospital, London, United Kingdom.

[3]Medical Nuclear Magnetic Resonance Facility, University of Iowa Roy J. and Lucille A. Carver College of Medicine, B291 Carver Biomedical Research Building, 285 Newton Road, Iowa City, IA 52242, USA

[4]National Institute for Health Research Great Ormond Street Hospital Biomedical Research Centre, UCL Great Ormond Street Institute of Child Health, London, United Kingdom.

[5]The State Key Laboratory of Protein and Plant Gene Research, School of Life Sciences, Academy for Advanced Interdisciplinary Studies, Peking-Tsinghua Center for Life Sciences, Peking University, Beijing, 100871, China

[6]Department of Pharmacology, Department of Cellular and Molecular Medicine, Department of Chemistry and Biochemistry, University of California, San Diego, La Jolla, CA 92093, USA

* Corresponding author

Abstract

Matriglycan [-GlcA-β1,3-Xyl-α1,3-]$_n$ serves as a scaffold in many tissues for extracellular matrix proteins containing laminin-G domains including laminin, agrin, and perlecan. Like-acetylglucosaminyltransferase-1 (LARGE) synthesizes and extends matriglycan on α-dystroglycan (α-DG) during skeletal muscle differentiation and regeneration; however, the mechanisms which regulate matriglycan elongation are unknown. Here, we show that *Protein O-Mannose Kinase (POMK)*, which phosphorylates mannose of core M3 (GalNac-β1,3-GlcNac-β1,4-Man) preceding matriglycan synthesis, is required for LARGE-mediated generation of full-length matriglycan on α-DG (~150 kDa). In the absence of *POMK*, LARGE synthesizes a very short matriglycan resulting in a ~90 kDa α-DG in mouse skeletal muscle which binds laminin but cannot prevent eccentric contraction-induced force loss or muscle pathology. Solution NMR spectroscopy studies demonstrate that LARGE directly interacts with core M3 and binds preferentially to the phosphorylated form. Collectively, our study demonstrates that phosphorylation of core M3 by *POMK* enables LARGE to elongate matriglycan on α-DG, thereby preventing muscular dystrophy.

Introduction

The extracellular matrix (ECM) is essential for development, regeneration and physiological function in many tissues, and abnormalities in ECM structure can lead to disease (***Rowe et al., 2008; Hudson et al., 2003***). The heteropolysaccharide [-GlcA-β1,3-Xyl-α1,3-]$_n$ (called matriglycan) is a scaffold for ECM proteins containing laminin-G (LG) domains (e.g. laminin, agrin, and perlecan) (***Yoshida-Moriguchi et al., 2015; Hohenester, 2019; Michele et al, 2002; Ohtsubo et al., 2006***) and has the remarkable capacity to be tuned during skeletal muscle development and regeneration (***Goddeeris et al., 2013***). Over eighteen genes are involved in the synthesis of the post translational modification terminating in matriglycan (***Figure 1***), and defects in this process cause dystroglycanopathies, congenital and limb-girdle muscular dystrophies that can be accompanied by brain and eye defects. Like-acetylglucosaminyltransferase-1 (LARGE), synthesizes matriglycan on the cell-surface glycoprotein, α-dystroglycan (α-DG) (***Inamori et al., 2012***). Addition of matriglycan enables α-DG to serve as the predominant ECM receptor in skeletal muscle and brain (***Yoshida-Moriguchi et al., 2015; Hohenester, 2019; Jae et al., 2013; Yoshida-Moriguchi et al., 2010; Yoshida-Moriguchi et al., 2013)***. Crystal structure studies have shown that a single glucuronic acid-xylose disaccharide (GlcA-Xyl) repeat binds to laminin-α2 LG4 domain (***Briggs et al., 2016; Hohenester et al., 1999***), and there is a direct correlation between the number of GlcA-Xyl repeats on α-DG and its binding capacity for ECM ligands (***Goddeeris et al., 2013; Inamori et al., 2012)***. During skeletal muscle differentiation, LARGE elongates matriglycan to its full length for normal skeletal muscle function (***Goddeeris et al., 2013)***. However, little is known about the mechanisms which control matriglycan elongation.

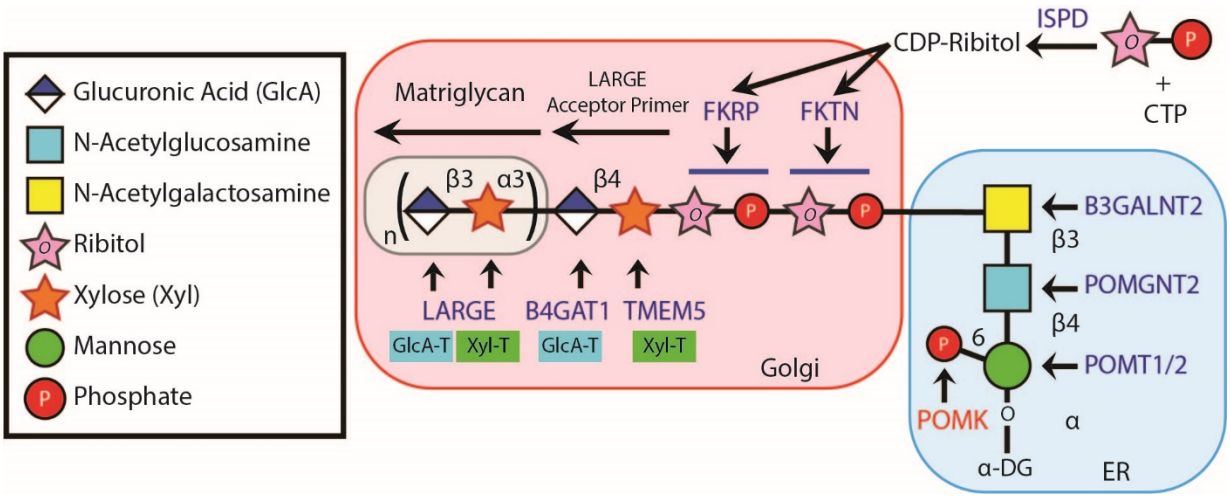

Figure 1. Synthesis of the α-DG Laminin-Binding Modification and Enzymes Involved. Synthesis of the laminin-binding modification begins with the addition of the core M3 trisaccharide (GalNac-β3-GlcNac-β4-Man) on α-DG by the sequential actions of Protein *O*-Mannosyltransferase-1 and 2 (POMT1/2), Protein *O*-linked mannose *N*-acetylglucosaminyltransferase 2 (POMGNT2), and β1,3-*N*-acetylgalactosaminyltransferase 2 B3GALNT2, in the ER. POMK phosphorylates the C6 hydroxyl of mannose after synthesis of core M3. The phosphorylated core M3 is further elongated in the Golgi by Fukutin (FKTN), Fukutin-Related Protein (FKRP), Transmembrane Protein 5 (TMEM5), β1-4-glucuronyltransferase-1 (B4GAT1), and Like-acetylglucosaminyltranserase-1 (LARGE). Isoprenoid Synthase Domain-Containing (ISPD) produces cytidine diphosphate (CDP)-Ribitol in the cytosol, and this serves as a sugar donor for the reactions catalyzed by FKTN and FKRP. LARGE synthesizes matriglycan, which directly interacts with the LG domains of matrix ligands.

Complete loss-of-function mutations in the dystroglycanopathy genes abrogate synthesis of the post translational modification terminating in matriglycan. Such mutations preclude addition of matriglycan and, thereby, cause the most severe form of dystroglycanopathy, Walker-Warburg Syndrome (WWS), which is lethal *in utero* or within a day or two of birth **(*Yoshida-Moriguchi et al., 2015; Hohenester, 2019; Michele et al., 2002; Ohtsubo et al., 2006*)**. Protein *O*-Mannose Kinase (POMK) is a glycosylation-specific kinase that phosphorylates mannose of the core M3 trisaccharide (GalNac-β1,3-GlcNac-β1,4-Man) during synthesis of the *O*-mannose-linked polysaccharide ending in matriglycan **(*Yoshida-Moriguchi et al., 2015; Hohenester et al., 2019; Jae et al., 2013; Yoshida-Moriguchi et al., 2013; Zhu et al., 2016*)**. Interestingly, unlike with other dystroglycanopathy genes there are patients with complete loss-of-function mutations in POMK who suffer from mild forms of dystroglycanopathy **(*Di Costanzo et al., 2014; von Renesse et al., 2014*)**, suggesting some expression of matriglycan without POMK. Here, we have used a multidisciplinary approach to show that phosphorylation of core M3 by POMK is not necessary for the LARGE-mediated synthesis of a short, non-extended form of matriglycan on α-DG (~90 kDa) with reduced laminin binding capacity; however, POMK is required for LARGE to generate full-length matriglycan on α-DG (~150 kDa). In the absence of the phosphorylated core M3, the non-extended matriglycan on ~90 kDa α-DG binds laminin and maintains specific force but cannot prevent eccentric contraction-induced force loss or skeletal muscle pathology. Furthermore, solution NMR studies demonstrated that LARGE directly interacts with core M3, binding preferentially to the phosphorylated form. Therefore, our study shows that phosphorylation of core M3 by POMK enables LARGE to elongate matriglycan on α-DG. Collectively, our work demonstrates a requirement for POMK in the LARGE-mediated synthesis of full-length matriglycan and proper skeletal muscle function.

Results

To determine if matriglycan can be expressed in the absence of POMK function, and therefore better understand the role of POMK in matriglycan synthesis, we studied skeletal muscle from a patient (NH13-284) with a POMK (D204N) mutation (***Figure 2A***) and congenital muscular dystrophy (CMD) accompanied by structural brain malformations. D204 serves as the catalytic base in the phosphorylation reaction catalyzed by the kinase (***Figure 2A; Figure 2- Figure Supplement 1***) and its mutation is predicted to eliminate POMK activity (***Figure 2-Figure Supplement 1***) **(*Zhu et al., 2016*)**. POMK activity from skin fibroblasts and skeletal muscle of patient NH13-284 (POMK D204N) was undetectable when compared to control fibroblasts and muscle, respectively (***Figure 2B***). Fibroblast LARGE activity and skeletal muscle B4GAT1 activity of patient NH13-284 were similar to those of a control (***Figure 2-Figure Supplement 2A, 2B***). Immunofluorescence analyses of POMK D204N muscle demonstrated partial immunoreactivity to IIH6 (anti-matriglycan), while the transmembrane subunit of DG, β-DG, was expressed normally in POMK D204N muscle (***Figure 2C***). Flow cytometry using IIH6 also demonstrated partial immunoreactivity in POMK D204N fibroblasts (***Figure 2-Figure Supplement 2C***). To test the effect of the POMK mutation on ligand binding we performed a laminin overlay using laminin-111. Control human skeletal muscle showed the typical broad band of α-DG laminin binding centered at ~150 kDa range; in contrast, laminin binding at ~90 to 100 kDa range with reduced intensity was observed in POMK D204N skeletal muscle (***Figure 2D***).

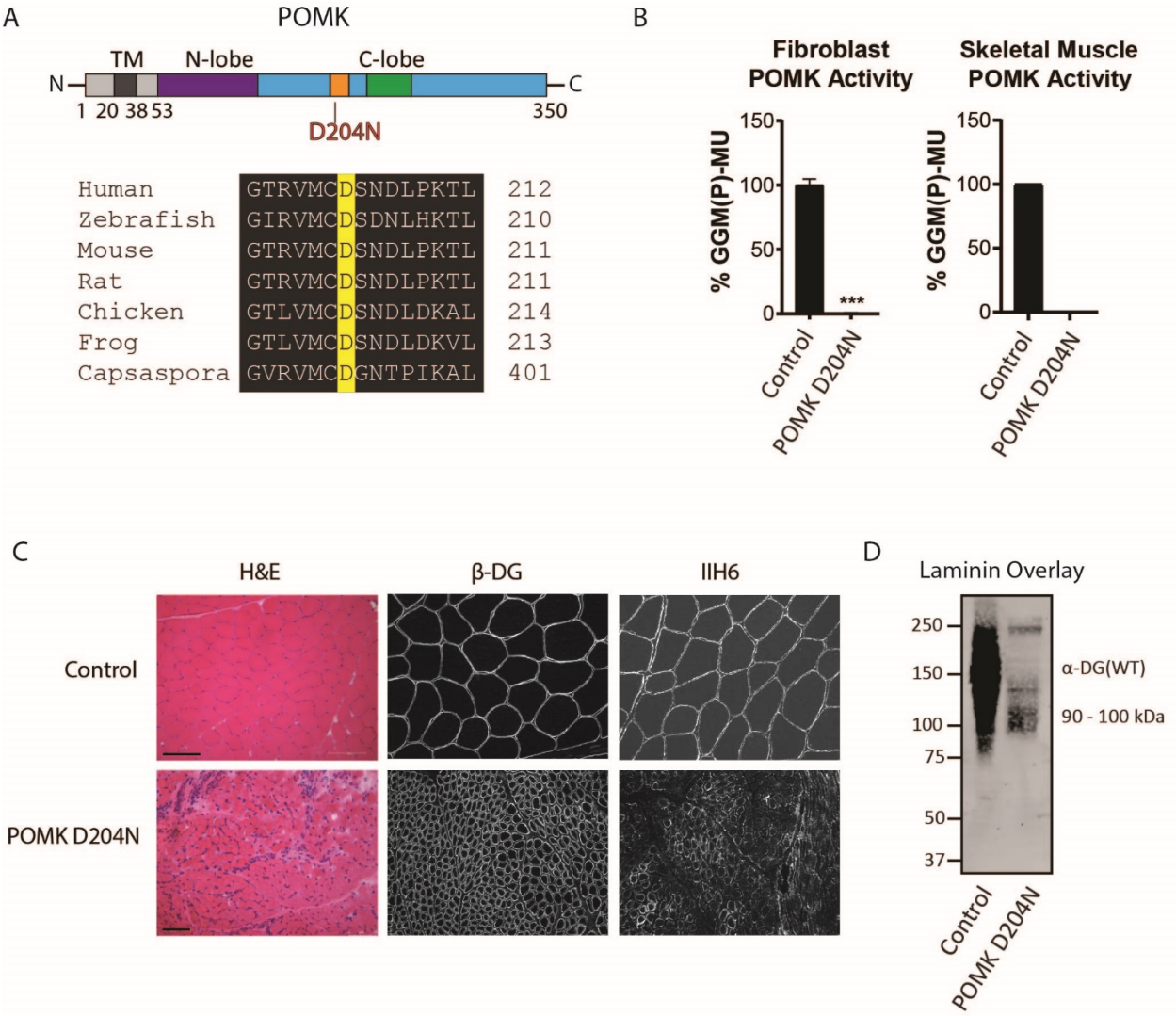

Figure 2. Characterization of a Patient with a Loss-of-Function Mutation in POMK. **A,** (above) Human POMK consists of a transmembrane domain (TM) and a kinase domain (N-lobe and C-lobe). The kinase domain contains the catalytic loop (orange) and activation segment (green). (below) Alignment of protein sequences flanking the D204N mutation. The mutation alters a highly conserved aspartate that is the catalytic base of the phosphorylation reaction catalyzed by the kinase. **B**, POMK activity in control and patient NH13-284 (POMK D204N) fibroblasts (left) and skeletal muscle (right). n=3 experiments were performed in fibroblasts. Triple asterisks: p-value<0.001. Due to limited skeletal muscle, n=1 experiment was performed. **C**, Histology and immunofluorescence of control and POMK D204N skeletal muscle using IIH6 (anti-matriglycan) and a β-DG antibody. (Scale bars: Control- 200 µM, POMK D204N- 75 µM). **D,** Laminin overlay of control and POMK D204N skeletal muscle.

To understand the biochemical basis of the ~90 to 100 kDa laminin binding in the absence of POMK activity, we targeted *POMK* using LoxP sites and Cre driven by the Muscle Creatine Kinase (MCK) promoter, or both the MCK promoter and the Paired Box 7 (Pax7) promoter (***Figure 3-Figure Supplement 1, 2***) (***Brüning et al., 1998; Keller et al., 2004***) to generate muscle-specific POMK null mouse models. Histologic analyses of MCK-Cre; Pax7-Cre; $POMK^{LoxP/LoxP}$ (M-POMK KO) quadriceps muscles revealed hallmarks of a mild muscular dystrophy (***Figure 3A***). Quadriceps muscle extracts of MCK-Cre; $POMK^{LoxP/LoxP}$ mice showed reduced POMK activity compared to $POMK^{LoxP/LoxP}$ muscle but had similar levels of LARGE activity (***Figure 3B, 3C***). M-POMK KO mice also showed reductions in 2-limb grip strength and body weight and elevations in post-exercise creatine kinase (CK) levels compared to littermate control $POMK^{LoxP/LoxP}$ mice (***Figure 3D; Figure 3-Figure Supplement 3***). Immunofluorescence analysis of M-POMK KO muscle showed that β-DG is expressed at the skeletal-muscle sarcolemma (***Figure 3A***); however, like patient NH13-284 IIH6 immunoreactivity persisted in M-POMK KO muscle, but at a reduced intensity (***Figure 3A***).

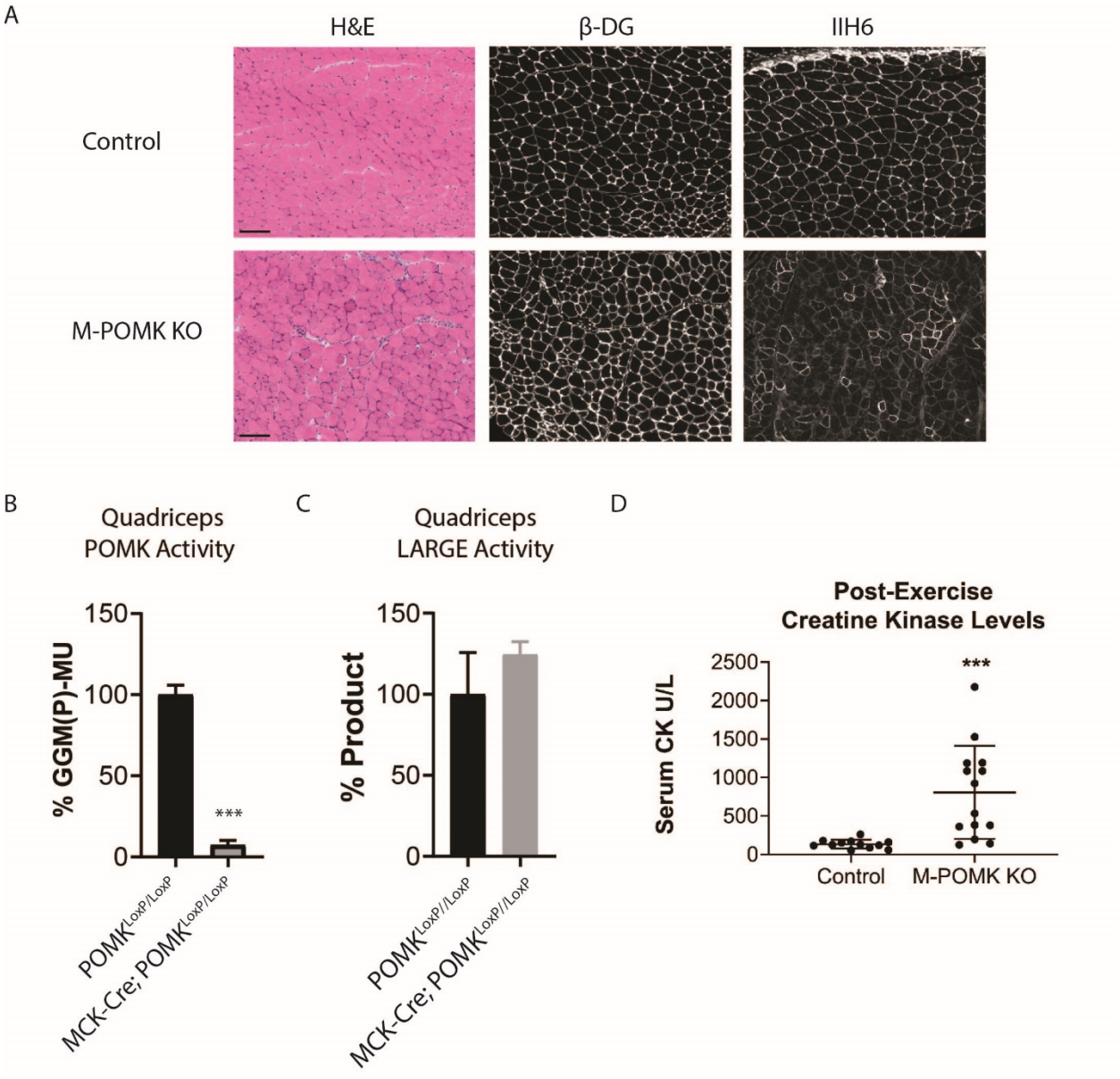

Figure 3. Mice with a Muscle-Specific Loss of POMK Develop Hallmarks of a Mild Muscular Dystrophy. **A**, H&E and immunofluorescence analyses using IIH6 (anti-matriglycan) and an anti-β-DG antibody of quadriceps muscles of 4-6-week-old $POMK^{LoxP/LoxP}$ (control) and MCK-Cre; Pax7-Cre $POMK^{LoxP/LoxP}$ (M-POMK KO) mice. Scale bars: 100 µM. **B,** POMK and **C,** LARGE activity in extracts of MCK-Cre; $POMK^{LoxP/LoxP}$ and $POMK^{LoxP/LoxP}$ quadriceps skeletal muscles. Triple asterisks indicate statistical significance using a Student's unpaired t-test with a p-value<0.0001 (three replicates). **D,** Creatine kinase levels of 8-week old M-POMK KO and control mice. P-values were calculated with Student's unpaired t-test. Triple asterisks: p-value < 0.05.

We next examined *ex vivo* force production in extensor digitorum muscles (EDL) muscles of 18-20 week-old control and M-POMK KO mice. EDL muscle mass and cross-sectional area (CSA) were reduced in M-POMK KO mice compared to control mice (***Figure 4A, 4B***). Additionally, M-POMK KO EDL absolute isometric tetanic force production was significantly lower than that of controls (***Figure 4C***). However, when normalized to muscle CSA, force production was comparable to control values (***Figure 4D***). We also sought to determine if M-POMK KO muscle could withstand repeated eccentric contractions. EDL muscles of M-POMK KO mice demonstrated greater force deficits after five and eight lengthening contractions (LC) and recovered to a lower level after 45 minutes compared to control EDL (***Figure 4E***). Together, the isometric and eccentric contractile studies suggest that the M-POMK KO EDL muscles display a specific force similar to controls (***Figure 4D***); however, muscle integrity is compromised following the stress of repeated eccentric contractions, as displayed by the slow, but progressive decline in force production and hampered recovered ***(Figure 4E)***. Thus, the current results demonstrate that the short matriglycan in POMK-deficient skeletal muscle can maintain specific force, but cannot prevent eccentric contraction-induced force loss or muscle pathology.

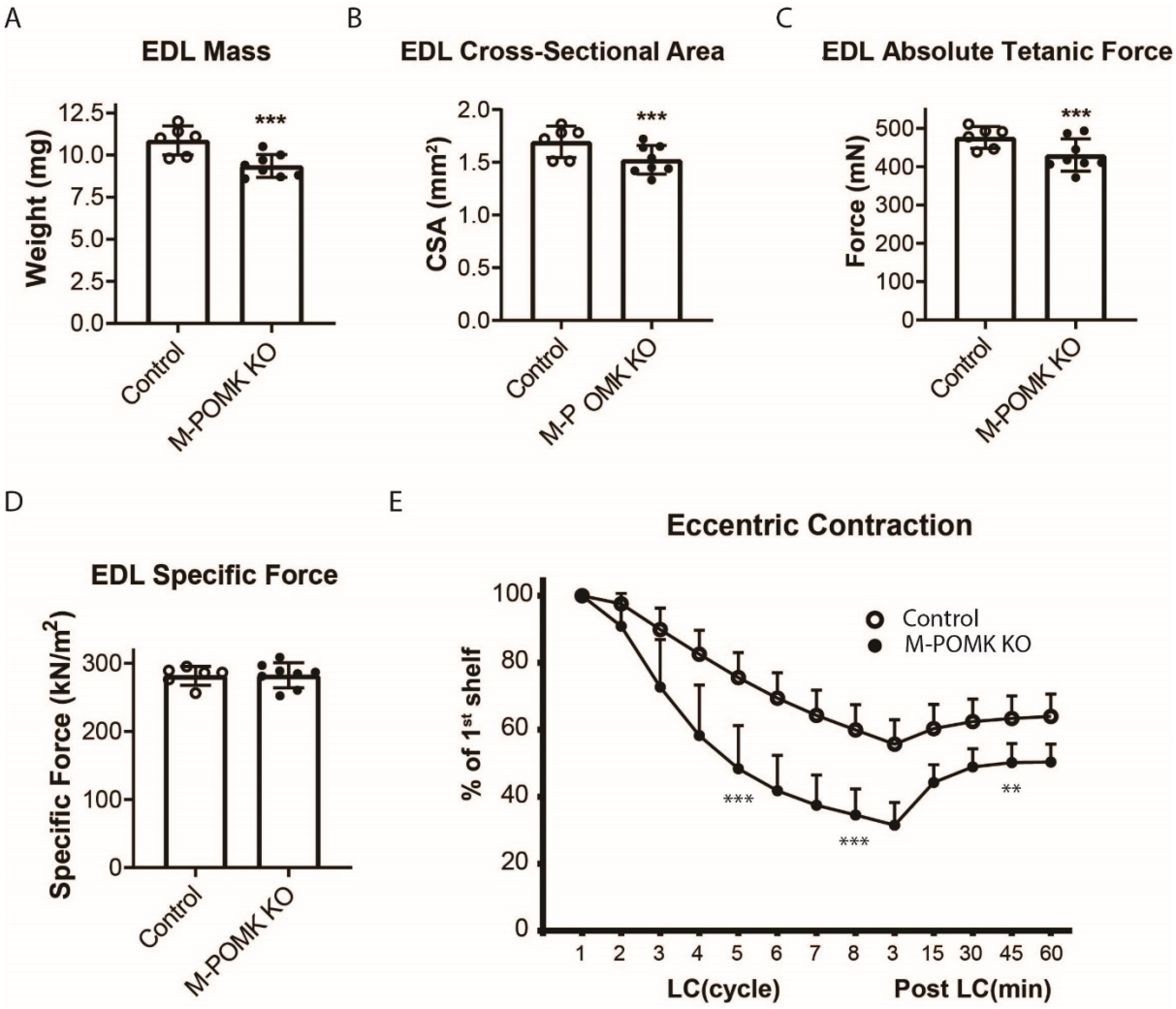

Figure 4. MCK-Cre; Pax7-Cre; POMK$^{LoxP/LoxP}$ EDL Demonstrates Eccentric Contraction-Induced Force Loss. **A,** Mass (milligrams) of POMK$^{LoxP/LoxP}$ (Control) and MCK-Cre; Pax7-Cre; POMK$^{LoxP/LoxP}$ (M-POMK KO) EDL muscles tested for force production. ***Statistical significance with Student's unpaired t-test at p-value<0.05 (p=0.0031). **B,** Cross-sectional area (CSA) of EDL muscles. ***Statistical significance using Student's unpaired t-test with p-value<0.05 (p=0.0463). **C,** Maximum Absolute Tetanic Force production by Control and M-POMK KO EDL muscles. ***Statistical significance using Student's unpaired t-test with a p-value<0.05 (p=0.0395). **D,** Specific Force Production in Control and M-POMK KO extensor digitorum longus (EDL) muscles. (p=0.921). **E**, Force deficit and force recovery in POMK$^{LoxP/LoxP}$ (Control, n=3 mice) and (M-POMK KO, n=4 mice) mice after eccentric contractions. Individual extensor digitorum longus (EDL) muscles from 18-20-week-old male mice were tested and are represented by open (Control) or closed (M-POMK KO) circles. ***Statistical significance using Student's unpaired t-test with a p-value<0.001 compared to Control EDL at given LC cycle. **Statistical significance using Student's unpaired t-test with a p-value=0.0027 compared to Control EDL at given LC cycle. Error bars represent SD.

Biochemical analysis of control and M-POMK KO muscle showed a typical, lower molecular weight (MW) α-DG with anti-core DG antibody (***Figure 5A***), however, on laminin overlay, we observed laminin binding at 90-100 kDa (***Figure 5B***), similar to POMK D204N skeletal muscle (***Figure 2D***). IIH6 also showed binding at 90-100 kDa (***Figure 5C***). Solid-phase binding analyses of M-POMK KO and MCK-Cre; $POMK^{LoxP/LoxP}$ skeletal muscle demonstrated a reduced binding capacity (relative B_{max}) for laminin-111 compared to control muscle (***Figure 5-Figure Supplement 1A***), but higher than that of $LARGE^{myd}$ muscle, which lacks matriglycan due to a deletion in *LARGE*.

To determine if matriglycan is responsible for the laminin binding at 90-100 kDa in POMK-null muscle, we treated glycoproteins enriched from skeletal muscles of M-POMK KO and MCK-Cre; $POMK^{LoxP/LoxP}$ mice with two exoglycosidases, α-Xylosidase and β-Glucuronidase, which in combination digest matriglycan (***Figure 5-Figure Supplement 1B, 2A, 2B***) (***Briggs et al., 2016***). Laminin overlay and solid phase analysis showed a reduction in laminin binding from these muscles after dual exoglycosidase digestion (***Figure 5D, 5E; Figure 5- Figure Supplement 2A, 2B***).

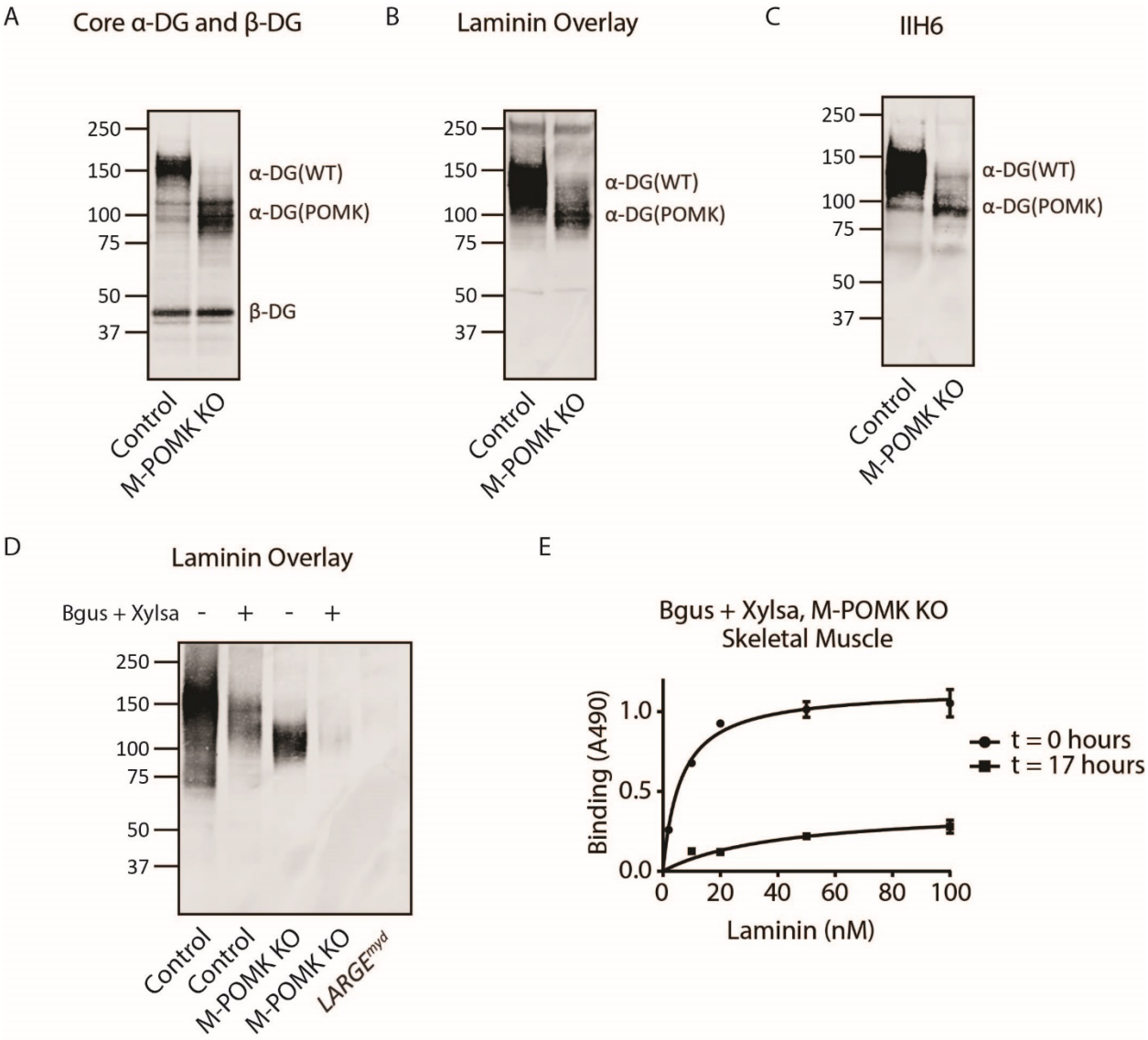

Figure 5. Mice with a Muscle-Specific Loss of POMK Express Matriglycan. **A**, Biochemical analysis of Control and M-POMK KO skeletal muscle. Glycoproteins were enriched from quadriceps skeletal muscles of mice using wheat-germ agglutinin (WGA)-agarose. Immunoblotting was performed with antibody AF6868, which recognizes core α-DG and β-DG (three replicates). **B**, Laminin overlay of quadriceps muscles of Control and M-POMK KO mice (three replicates). **C,** IIH6 immunoblotting of Control and M-POMK KO quadriceps muscle. **D, E,** Laminin overlay (**D**) and Solid phase analysis (**E**) of skeletal muscles of M-POMK KO mice treated in combination with two exoglycosidases, α-xylosidase (Xylsa) and β-glucuronidase (Bgus) for 17 hours (three replicates).

To study the role of POMK further, we used *POMK* KO HAP1 cells, which have undetectable levels of POMK activity and expression (***Figure 6A; Figure 6- Figure Supplement 1A***) (***Zhu et al., 2016***). A mass spectrometry (MS)-based glycomic analysis of *O*-glycans carried by recombinantly-expressed DG mucin-like domain indicated the absence of an MS peak at *m/z* 873.5 corresponding to phosphorylated core M3 *O*-glycan (***Figure 6D, 6E***), consistent with an undetectable level of POMK activity in *POMK* KO HAP1 cells. Compared to WT HAP1 cells, immunoblots of *POMK* KO HAP1 cells showed a reduction in IIH6 immunoreactivity, a decrease in MW of core α-DG, and the presence of laminin binding at ~90 kDa on laminin overlay (***Figure 6C; Figure 6-Figure Supplement 1B, 1C***). Laminin binding on overlay was rescued only after adenoviral transduction with wild-type (WT) POMK (POMK WT), but not with POMK containing D204N (POMK D204N) or D204A (POMK D204A) mutations (***Figure 6C***). POMK D204N also lacked POMK activity *in vitro* but showed normal B4GAT1, B3GALNT2, and LARGE activity, thus confirming the pathogenicity of the D204N mutation (***Figure 6A, 6B; Figure 6- Figure Supplement 1D, 1E***).

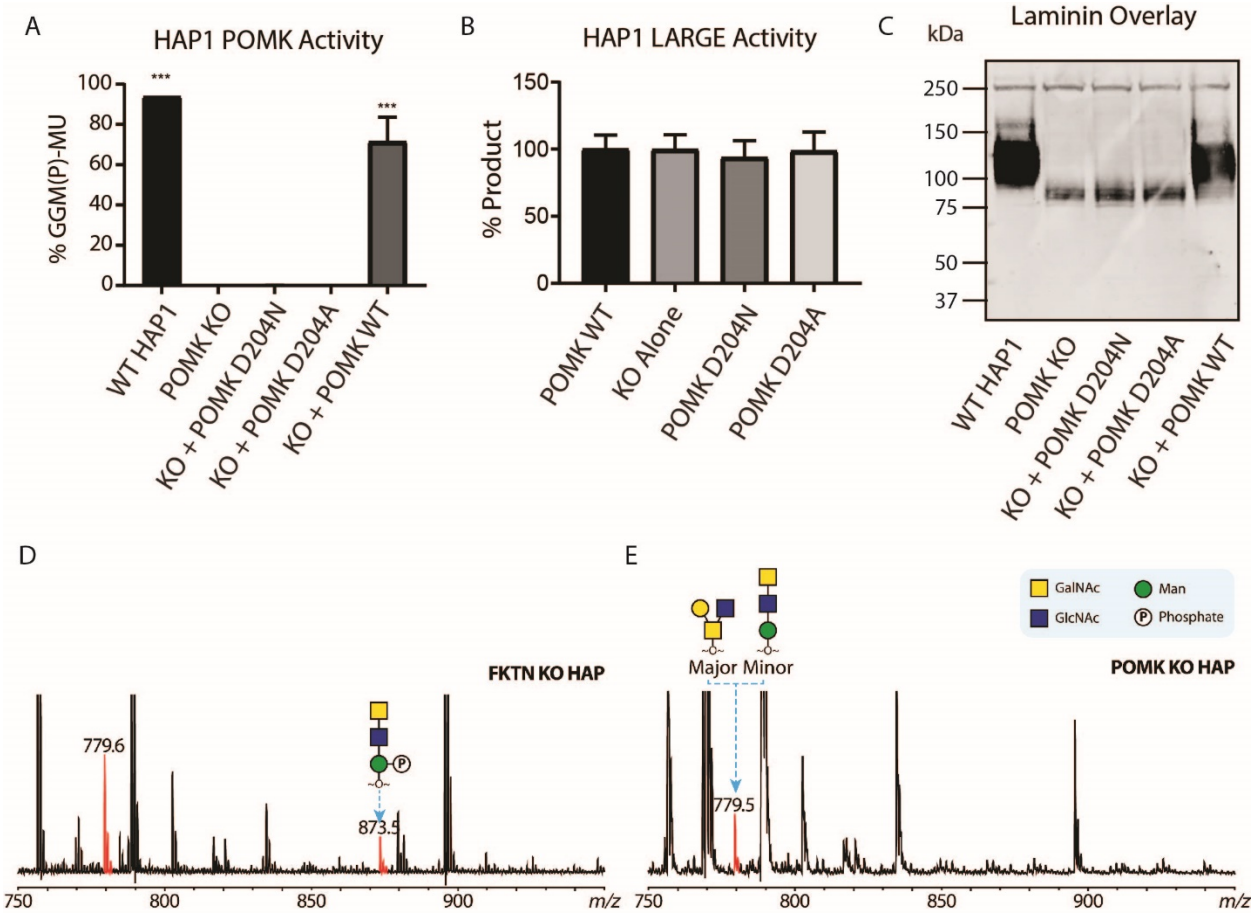

Figure 6. POMK D204N lacks Catalytic Activity. **A,** POMK or **B**, LARGE activity in *POMK* KO HAP1 cells transduced with adenoviruses encoding POMK D204N, D204A, or POMK WT. Asterisks: P-value<0.001 compared to *POMK* KO alone using One-Way ANOVA with Dunnett's Test for Multiple Comparisons (three replicates). **C**, Laminin overlay of *POMK* KO HAP1 cells expressing the indicated POMK mutants. **D**, **E,** Mass Spectrometry (MS)-based *O*-glycomic analyses of DG mucin-like domain (DG390TevHis) expressed in *Fukutin (FKTN)* (**D**) or *POMK* (**E**) KO HAP1 cells. *O*-glycans were released from the protein backbone and permethylated prior to Matrix-Assisted Laser Desorption/Ionization time-of-flight (MALDI-TOF) analyses. MS peaks at *m/z* 779.5 (779.6) correspond to a mixture of core 2 and core M3 *O*-glycan, and at 873.5, phosphorylated core M3 *O*-glycan (red).

To directly test if LARGE is required for synthesis of the 90 kDa laminin-binding glycoprotein in *POMK* KO HAP1 cells, we studied *POMK/LARGE* KO HAP1 cells, which bear a CRISPR/Cas9-mediated deletion in *LARGE* as well as *POMK*. *POMK/LARGE* KO HAP1 cells demonstrated the absence of the laminin binding at 90 kDa (***Figure 7A; Figure 7-Figure Supplement 1A, 1B***), indicating that LARGE is required for the synthesis of the matriglycan responsible for laminin binding at 90 kDa. Moreover, *POMK/DG* KO HAP1 cells demonstrated a complete absence of laminin binding (***Figure 7A***) and IIH6 immunoreactivity at 90 kDa (***Figure 7- Figure Supplement 1C***), demonstrating that α-DG is the glycoprotein that binds laminin in the absence of POMK. We, therefore, refer to this glycoprotein as POMK-null α-DG (α-DG(POMK)). Since the length of matriglycan correlates with its binding capacity for ECM ligands **(*Goddeeris et al., 2013*)**, we hypothesized that, given the MW of α-DG(POMK) at 90 kDa, the glycan must be shorter than full-length matriglycan, and therefore, have a lower B_{max} for laminin. We measured the binding capacity of HAP1 α-DG using solid-phase binding assays. B_{max} of α-DG(POMK) for laminin-111 was reduced compared to wild-type α-DG (α-DG(WT)) but was greater than that of α-DG from *LARGE* KO HAP1 cells (***Figure 7B***). *POMK/DG* KO HAP1 cells showed a reduction in B_{max} compared to *POMK* KO HAP1 cells, but similar to the low levels observed in *LARGE* KO HAP1 cells (***Figure 7B***). These data indicate that a short, non-extended form of matriglycan is synthesized on α-DG(POMK), and this short form has a lower binding capacity for laminin-111, thus exhibiting a reduced level of α-DG receptor function.

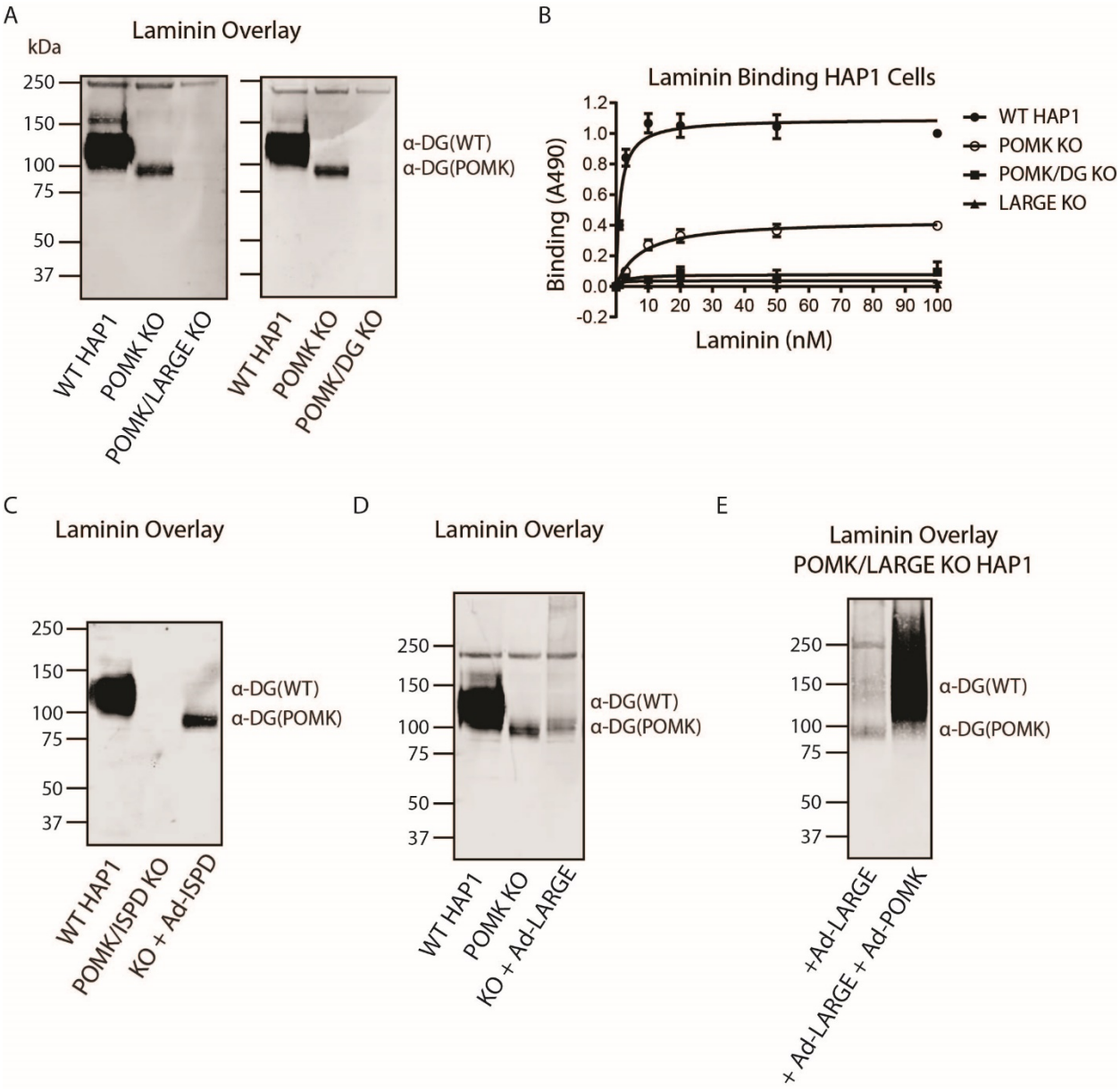

Figure 7. LARGE requires POMK to Elongate Matriglycan. **A**, WT, *POMK* KO, and *POMK/LARGE* KO HAP1 cells (left) or *POMK/DG* KO HAP1 cells (right) (three replicates). **B,** Solid phase analysis of WT and *POMK*, *POMK/DG*, and *LARGE* KO HAP1 cells (three replicates). **C, D, E**, Laminin overlays of the following KO HAP1 cells (three replicates): *POMK/ISPD* expressing Ad-*ISPD* (**C**); *POMK* expressing Ad-*LARGE* (**D**); *POMK/LARGE* expressing Ad-*LARGE* with or without Ad-*POMK* (**E**).

After POMK phosphorylates core M3, Fukutin (FKTN) modifies GalNac with ribitol-phosphate for synthesis of full-length matriglycan (***Figure 1***) **(*Yoshida-Moriguchi et al., 2015; Hohenester, 2019; Kanagawa et al., 2016*)**. Overexpression in *POMK* KO HAP1 cells of Isoprenoid Synthase Domain-Containing (ISPD), which synthesizes the substrate (CDP-ribitol) of FKTN (***Figure 1***), increases the amount of matriglycan (without changing its MW) responsible for laminin binding at 90 kDa (***Figure 7-Figure Supplement 2A, 2B, 2C***) **(*Willer et al., 2012; Gerin et al., 2016; Riemersma et al., 2015*)**. HAP1 cells lacking both POMK and ISPD do not express matriglycan, and adenoviral transduction of these cells with *ISPD* restores the 90 kDa laminin binding (***Figure 7C; Figure 7- Figure Supplement 2D, 2E***). FKTN overexpression in *POMK* KO HAP1 cells also increased the 90 kDa laminin binding (***Figure 7- Figure Supplement 3A, 3B, 3C***). These experiments collectively support a requirement for CDP-ribitol for synthesis of the non-extended form of matriglycan. This synthesis also requires the N-terminal domain of α-DG (DGN) **(*Hara et al., 2011; Kanagawa et al., 2004*)**, as a DG mutant lacking the DGN (DGE) expressed in *POMK/DG* KO HAP1 cells did not show laminin binding at 90 kDa (***Figure 7-Figure Supplement 4A, 4B, 4C***). Similar experiments also indicated that synthesis of the non-extended matriglycan in HAP1 cells requires threonine-317 of the mucin-like domain of α-DG (***Figure 7-Figure Supplement 4A, 4B, 4C***).

Overexpression of LARGE can rescue the defect in matriglycan synthesis in distinct forms of CMD as well as in *LARGE* KO HAP1 cells by generating very high molecular weight matriglycan (***Figure 7-Figure Supplement 5A***) **(*Barresi et al., 2004*)**. However, overexpression of LARGE in *POMK* or *POMK/LARGE* KO HAP1 cells did not produce very high molecular weight matriglycan (***Figure 7D, 7E; Figure 7- Figure Supplement 5B, 5C, 5D***). Only the rescue of *POMK/LARGE* KO HAP1 cells with POMK enabled LARGE to synthesize high molecular

weight matriglycan (***Figure 7E; Figure 7- Figure Supplement 5D***). These findings indicate that LARGE requires phosphorylated core M3 to extend matriglycan on α-DG to its mature and high molecular weight forms.

To understand why phosphorylated core M3 is needed for LARGE to elongate matriglycan, we measured the binding affinity of LARGE, as well as POMK, for the phosphorylated core M3 using solution NMR. We previously showed that the unphosphorylated core M3 binds to POMK with high affinity **(*Zhu et al., 2016*)**. The mannose anomeric proton (Man H1) is well resolved and its intensity decreases only slightly with increasing POMK protein concentration (***Figure 8-Figure Supplement 1A***). By fitting the intensity changes of the Man H1 peak as a function of POMK concentration, we obtained a dissociation constant of > 500 μM (***Figure 8C; Figure 8-Figure Supplement 1A, 1B***). These results indicate that, compared to the unphosphorylated core M3 of GGM-MU, the phosphorylated core M3 of GGMp-MU binds to POMK with a much weaker affinity. Then, we measured the binding affinities of LARGE for GGMp-MU and GGM-MU in a similar manner. Our results showed that LARGE binds with greater affinity to GGMp-MU compared to GGM-MU (K_d = 11.5±1.2 μM for GGMp-MU compared to K_d > 90 μM for GGM-MU) (***Figure 8A, 8B, 8D***). This indicates that the core M3 phosphate increases the binding affinity of LARGE for core M3 and could explain the ability of LARGE to elongate matriglycan in the presence of POMK.

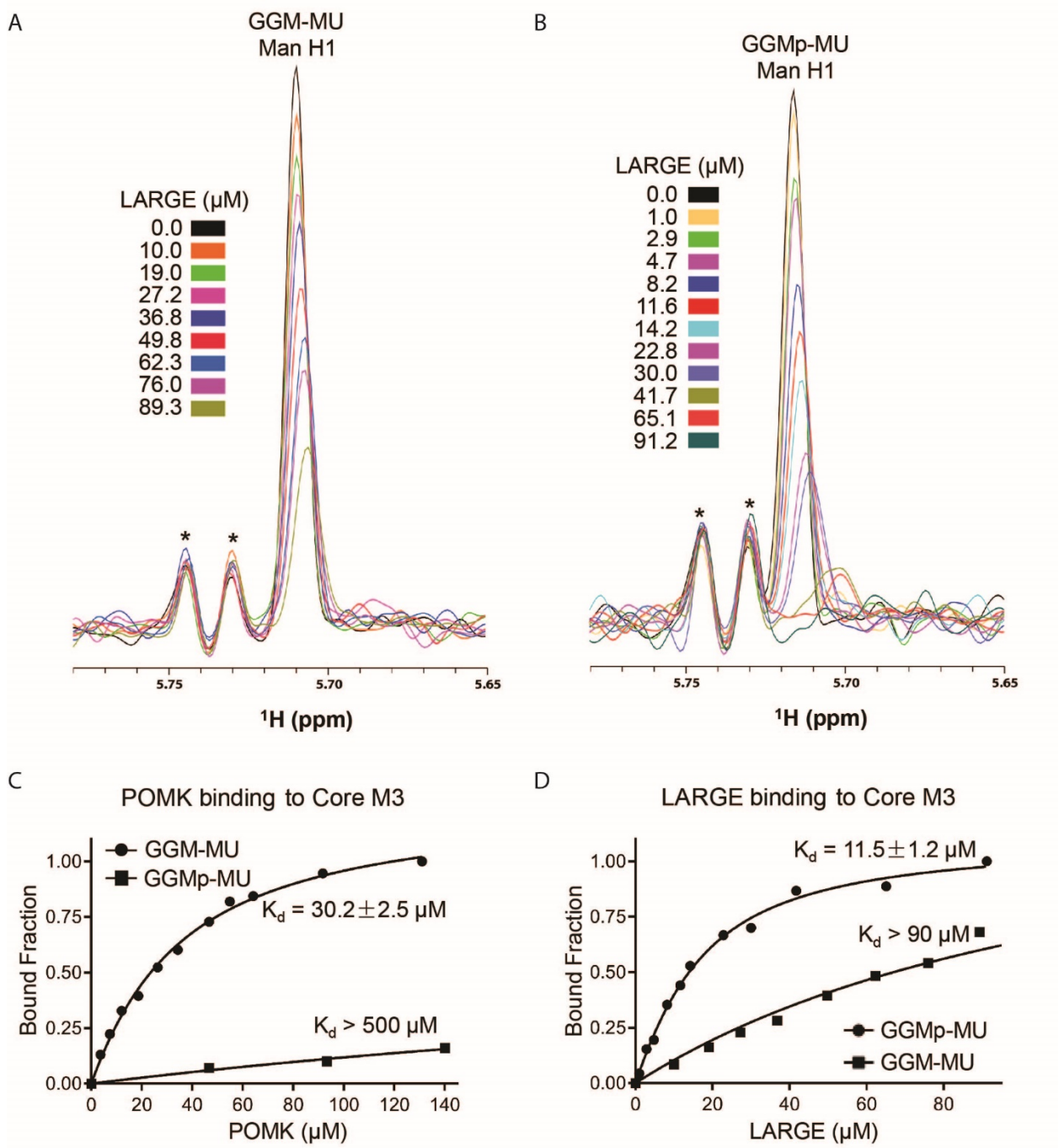

Figure 8. NMR Analyses of POMK and LARGE Binding to GGM-MU and GGMp-MU. **A, B,** 1D ^{1}H NMR spectra of the anomeric region of GGM-MU and GGMp-MU, respectively, were acquired for the glycan concentration of 10.0 μM in the presence of various concentrations of LARGE as indicated. The peak Man H1 is derived from the mannose anomeric H1 proton. Stars indicate impurity peaks derived from buffer. **C, D,** Fitting of the NMR binding data of POMK (**C**) and LARGE (**D**) to core M3 glycans of GGM-MU and GGMp-MU, respectively. The bound fraction was obtained from the NMR titration data by measuring the difference in the peak intensity of the anomeric proton Man H1 in the absence (free form) and presence (bound form) of POMK or LARGE, then divided by the peak intensity of the free form.

Discussion

POMK is a novel muscular dystrophy gene that phosphorylates mannose of the core M3 trisaccharide (GalNac-β1,3-GlcNac-β1,4-Man) on α-DG during synthesis of the *O*-mannose-linked polysaccharide ending in matriglycan. LARGE is responsible for the synthesis of matriglycan, and addition of matriglycan enables α-DG to serve as a predominant ECM receptor in many tissues, in particular, skeletal muscle and brain. Over eighteen genes are implicated in matriglycan synthesis, and complete loss-of-function mutations in these genes abrogate synthesis of the *O*-mannose linked modification and preclude the addition of matriglycan, thereby leading to dystroglycanopathies, congenital and limb-girdle muscular dystrophies with or without structural brain and eye abnormalities. Here, we have used a multidisciplinary approach to show that the absence of POMK activity does not preclude addition of matriglycan. Instead, in the absence of core M3 phosphorylation by POMK, LARGE synthesizes a very short, non-extended form of matriglycan on α-DG (~90 kDa); however, in order to generate full-length mature matriglycan on α-DG (~150 kDa), LARGE requires phosphorylation of core M3 by POMK **(*Figure 8- Figure Supplement 2A, 2B).***

Our study shows that the short form of matriglycan is able to bind to laminin with high affinity and thus enables α-DG (POMK) to function as an ECM receptor. Given the very small increase in apparent MW in α-DG(POMK) compared to α-DG from cells and muscle lacking LARGE (***Figure 5-Figure Supplement 2A; Figure 7-Figure Supplement 1A; Figure 8-Figure Supplement 3A***), the short, non-extended form of matriglycan likely contains very few Xyl-GlcA repeats. However, it can still bind laminin since only a single Xyl-GlcA repeat is needed for laminin binding **(*Briggs et al., 2016*)** but it cannot function as an ECM scaffold. This short matriglycan likely attenuates muscular dystrophy in our patient with a complete loss-of-function

mutation in POMK, preventing the severe CMD phenotype that is observed in the complete absence of the other known dystroglycanopathy genes.

Muscle-specific POMK KO mice express the short, non-extended form of matriglycan on ~90 kDa α-DG and develop a mild muscular dystrophy phenotype. Muscle physiology studies demonstrate that the short matriglycan expressed in the absence of POMK can maintain specific force but cannot prevent eccentric contraction-induced force loss or skeletal muscle pathology. Interestingly, missense mutations in FKRP that cause LGMD2I also show reduced expression of matriglycan ***(Yoshida-Moriguchi et al., 2015)*** and exhibit a milder muscular dystrophy. Thus, M-POMK KO mice are an excellent model of milder forms of dystroglycanopathy in which short matriglycan is expressed and will be useful for future studies of these forms of dystroglycanopathy.

Biochemical studies using various POMK null HAP1 cell lines demonstrated that the synthesis of the short, non-extended form of matriglycan, like full-length matriglycan, requires LARGE, DGN, CDP-ribitol and threonine-317 of the mucin-like domain of α-DG. LARGE is known to interact with DGN, and this interaction is required for LARGE to modify α-DG during synthesis of full-length matriglycan ***(Kanagawa et al., 2004; Hara et al., 2011)***. Cell biological experiments demonstrated that LARGE can act on α-DG in the absence of the phosphorylated core M3 but requires DGN. The binding of LARGE to the DGN likely enables LARGE to generate the non-extended matriglycan on an acceptor oligosaccharide lacking phosphorylated core M3. Indeed, that threonine-317, closest to the DGN, is modified with the non-extended form of matriglycan further indicates the importance of the DGN for binding LARGE and enabling its function in the absence of phosphorylated core M3. Solution NMR studies reveal that LARGE has an increased binding affinity for core M3 when the core M3 mannose is phosphorylated, and the increased binding affinity of LARGE for the phosphorylated core M3 likely underlies the

ability of LARGE to synthesize full-length and high molecular weight matriglycan. The phosphorylated core M3, could therefore, serve to recruit LARGE, bound to DGN, to its acceptor oligosaccharide, where LARGE can generate full-length matriglycan. Taken together, these results indicate that LARGE requires DGN to synthesize the short, non-extended form of matriglycan but needs both the DGN and the phosphorylated core M3 to generate full-length matriglycan on α-DG.

Our study demonstrates that POMK is required for the synthesis of full-length and high-molecular weight forms of matriglycan ***(Figure 8- Figure Supplement 2A)*.** In the absence of POMK, LARGE generates a short, non-extended form of matriglycan ***(Figure 8- Figure Supplement 2B.*** Collectively, our work provides the first insights into the pathogenic mechanism behind POMK-deficient muscular dystrophy and better elucidates how full-length matriglycan is synthesized so it can act as a scaffold for ECM proteins, thereby enabling proper skeletal muscle function and preventing muscular dystrophy.

Methods

Patient Information Patient NH13-284 received a diagnosis of congenital muscular dystrophy (CMD) with brain malformations.

Generation of POMK$^{LoxP/LoxP}$ Mice

The *POMK* gene consists of five exons, exons 1, 2, and 3, which are non-coding and exons 4 and 5, which are coding (***Zhu et al., 2016; Di Costanzo et al., 2014***). We used Clustered Regularly Interspersed Short Palindromic Repeats (CRISPR)-Cas9 to insert LoxP sites around *exon 5*.

*POMK*_5P1 TTCTTTCTGTGATGTGTGCTTATTC
*POMK*_5P2 CAGACACTCACCCTTTACCTTAG
Wildtype: 197 bp
Targeted: 235 bp

*POMK*_3P1 AGCCACACCTTCCTACAGTC
*POMK*_3P2 AAGCTCTGCCCAGAGAGAAG
Wildtype: 123 bp
Targeted: 162 bp

*POMK*_5'_guide(601) CGTGTCCCGCCAGGAATGAA
*POMK*_3'_guide(3P1) TCAGGAGGCGGCTCCCAGTG

*POMK*_5'_donor(601; PAGE purified)
TCCTCATCTTCTCCCTGTGCAGTCAATCTGCACAGCTCCCTGCACACATGGCTTATAG
AGTGGTTCTCACCCCGCCCTTCATAACTTCGTATAGCATACATTATACGAAGTTATG
GTACCTCCTGGCGGGACACGAATAAGCACACATCACAGAAAGAAGTCTGTTGTCTT
GACTGCCCAGCCCTCCGCAGCTGCCACCC
*POMK*_3'_donor(3P1; PAGE purified)
AGTGTGAGATTCAAGTGTGGATATGCAGTGATCCTCTGGCCACACTTGTGAGCAGCC
ACACCTTCCTACAGTCCCTCACTATAACTTCGTATAGCATACATTATACGAAGTTATG
GATCCGGGAGCCGCCTCCTGAGCCCTGCTGTGTAACCCACCTACCTTCCCTCCTTTCA
CACTAGAAGCTGAGAGCTCTTCTCTTC

Animals

B6SJLF1/J mice were purchased from Jackson Labs (100012; Bar Harbor, ME). Male mice older than 8 weeks were used to breed with 3-5-week-old super-ovulated females to produce zygotes for electroporation. Female ICR (Envigo, Indianapolis, IN; Hsc:ICR(CD-1)) mice were used as

recipients for embryo transfer. All animals were maintained in a climate-controlled environment at 25°C and a 12/12 light/dark cycle. Animal care and procedures were approved by and conformed to the standards of the Institutional Animal Care and Use Committee of the Office of Animal Resources at the University of Iowa.

Preparation of Cas9 RNPs and the microinjection mix

Chemically modified CRISPR-Cas9 crRNAs and CRISPR-Cas9 tracrRNAs were purchased from Integrated DNA Technologies (IDT) (Alt-R® CRISPR-Cas9 crRNA; Alt-R® CRISPR-Cas9 tracrRNA (Cat# 1072532)). The crRNAs and tracrRNA were suspended in T10E0.1 and combined to 1 µg/µL (~29.5 µM) final concentration in a 1:2 (µg: µg) ratio. The RNAs were heated at 98°C for 2 minutes and allowed to cool slowly to 20°C in a thermal cycler. The annealed cr:tracrRNAs were aliquoted to single-use tubes and stored at -80°C.

Cas9 nuclease was also purchased from IDT (Alt-R® S.p. HiFi Cas9 Nuclease). Cr:tracr:Cas9 ribonucleoprotein complexes were made by combining Cas9 protein and each cr:tracrRNA; final concentrations: 60 ng/µL (~0.4 µM) Cas9 protein and 60 ng/µL (~1.7 µM) cr:tracrRNA). The Cas9 protein and annealed RNAs were incubated at 37°C for 10 minutes. The two RNP mixes were combined and incubated at 37°C for an additional 5 minutes. The single stranded oligonucleotide donors (ssODN) were purchased from IDT as Ultramers. The ssODNs were added to the RNPs and the volume adjusted to the final concentrations in the injection mix were 10 ng/µL each ssODN; 20 ng/µL each guide RNA and 40 ng/µL Cas9 Protein.

Collection of embryos and microinjection

Pronuclear-stage embryos were collected using previously described methods **(*Pinkert et al., 2002*)**. Embryos were collected in KSOM media (Millipore, Burlington, MA; MR101D) and washed 3 times to remove cumulous cells. Cas9 RNPs and ssODNs were injected into the pronuclei

of the collected zygotes and incubated in KSOM with amino acids at 37ºC under 5% CO2 until all zygotes were injected. Fifteen to 25 embryos were immediately implanted into the oviducts of pseudo-pregnant ICR females.

Insertion of loxP1 (5') and loxP2 (3') sites was confirmed by cloning and sequencing of genomic PCR products (Figure S2) from tail DNA of filial 0 (F0) $POMK^{LoxP/+}$ mice using primers flanking the 5' LoxP site, ACTCCAGTTGGTTTCAGGAAG and GAGGGAAGAGAAGTCAGGAAAG. For the 3' LoxP site, primers of sequence ACCGAGTGTGAGATTCAAGTG and GGTTGCTGGTAGGGTTAAGAG were used. The 5' LoxP site contains a *Kpn1* cleavage site, and the 3' LoxP site contains a *BamH1* site. The screen of the 5' LoxP site gives a product of 803 base pairs for the LoxP allele when uncut. *Kpn1* digestion of the 5' LoxP site gives 3 products of 381, 355, and 67 base pairs. A screen of the 3' LoxP site gives a product of 396 base pairs for the uncut allele with LoxP site, while *BamH1* digestion of the 3' LoxP site gives products of 273 and 123 base pairs.

Genotyping was carried out using primers flanking the exon 5 loxP1 site or the (TTCTTTCTGTGATGTGTGCTTATTC) or loxP2 (CAGACACTCACCCTTTACCTTAG) site. The wild-type allele is 197 bp while the floxed allele is 235 bp. $POMK^{LoxP/+}$ mice were backcrossed five generations onto a C57BL6/J background and backcrossed mice used whenever possible.

Mice expressing Cre under the Mouse Creatine Kinase (MCK) promoter, B6.FVB(129S4)-Tg(Ckmm-cre)5Khn/J (stock no. 006475) **(*Brüning et al., 1998*)** and the Pax7-Cre promoter, $Pax7^{tm1(cre)Mrc}$/J, (stock no. 010530) **(*Keller et al., 2004*)** were purchased from the Jackson Laboratory. Male mice expressing the MCK-Cre transgene were bred to female mice homozygous for the floxed *POMK* allele ($POMK^{LoxP/LoxP}$). Male F1 progeny with the genotype MCK-Cre; $POMK^{LoxP/+}$ were bred to female $POMK^{LoxP/LoxP}$ mice. A Cre PCR genotyping protocol was used

to genotype the Cre allele using standard Cre primers. The primers used were Sense: TGATGAGGTTCGCAAGAACC and Antisense: CCATGAGTGAACGAACCTGG.

Sanger sequencing of tail DNA was performed by the University of Iowa Genome Editing Core Facility to confirm incorporation of 5' and 3' LoxP sites. PCR probes were developed at Transnetyx to genotype mice expressing both Pax7-Cre and MCK-Cre. Genotyping of MCK-Cre; Pax7-Cre; POMK$^{LoxP/LoxP}$ mice was performed by Transnetyx using real-time PCR.

All mice were socially housed in a barrier-free, specific pathogen-free conditions as approved by the University of Iowa Animal Care and Use Committee (IACUC). Animal care, ethical usage, and procedures were approved and performed in accordance with the standards set forth by the National Institutes of Health and IACUC. For studies with MCK-Cre; POMK$^{LoxP/LoxP}$ mice, N=3 mice of each genotype (POMK$^{LoxP/LoxP}$ and MCK-Cre; POMK$^{LoxP/LoxP}$) were used. For studies with MCK-Cre; Pax7-Cre; POMK$^{LoxP/LoxP}$ mice, animals of varying ages were used as indicated, and N=3 each of POMK$^{LoxP/LoxP}$ and MCK-Cre; Pax7-Cre; POMK$^{LoxP/LoxP}$ were used. Littermate controls were employed whenever possible.

Forelimb Grip Strength Test

Forelimb grip strength was measured at 4 weeks of age. A mouse grip strength meter (Columbus Instruments, Columbus, OH) was mounted horizontally, with a nonflexible grid connected to the force transducer. The mouse was allowed to grasp the grid with its two front paws and then pulled away from the grid by its tail until the grip was broken. This was done three times over five trials, with a one-minute break between each trial. The gram force was recorded per pull, and any pull where only one front limb or any hind limbs were used were discarded. If the mouse turned, the pull was also discarded. After 15 pulls (5 sets of 3 pulls), the mean of the three highest pulls of the 15 was calculated and reported. Statistics were calculated using GraphPad Prism 8 software.

Student's T-Test was used (two-sided). Differences were considered significant at a p-value less than 0.05. Graph images were also created using GraphPad Prism and the data in the present study are shown as the means +/- SD unless otherwise indicated.

Creatine Kinase Assay

Creatine Kinase levels were measured in 8-week old mice 2 hours after mild downhill run (3 meters per minute for 5 minutes followed by 15 meters per minute for 10 minutes) at a 15- degree downhill incline. Blood was collected by tail vein bleeds from non-anesthetized, restrained mice using a Microvette CB300 (Sarstedt AG & Co, Newton, NC). Samples were centrifuged at 12,000 rpm for 10 minutes and prepared using an enzyme-coupled CK kit (Stanbio Laboratory, Boerne, TX) using the manufacturer's instructions. Absorbance was measured using a plate reader at 340 nm every 30 seconds for 2 minutes at 37°C. Statistics were calculated using GraphPad Prism software and Student's T-Test was used (two-sided). Differences were considered significant at a p-value less than 0.05. Graph images were also created using GraphPad Prism 8 and the data in the present study are shown as the means +/- SD unless otherwise indicated.

Body Weight Measurements

Mice were weighed after measuring grip strength using a Scout SPX222 scale (OHAUS Corporation, Parsippany, NJ), and the tester was blinded to genotype. Statistics were calculated using GraphPad Prism 8 software and Student's T-Test was used (two-sided). Differences were considered significant at a p-value less than 0.05. Graph images were also created using GraphPad Prism and the data in the present study are shown as the means +/- SD unless otherwise indicated.

Measurement of *in vitro* muscle function

To compare the contractile properties of muscles, extensor digitorum longus (EDL) muscles were surgically removed as described previously (***Rader et al., 2016***). The muscle was immediately placed in a bath containing a buffered physiological salt solution (composition in mM: NaCl, 137; KCl, 5; CaCl2, 2; MgSO4, 1; NaH2PO4, 1; NaHCO3, 24; glucose, 11). The bath was maintained at 25°C, and the solution was bubbled with 95% O_2 and 5% CO_2 to stabilize pH at 7.4. The proximal tendon was clamped to a post and the distal tendon tied to a dual mode servomotor (Model 305C; Aurora Scientific, Aurora, ON, Canada). Optimal current and whole muscle length (L_0) were determined by monitoring isometric twitch force. Optimal frequency and maximal isometric tetanic force (F_0) were also determined. The muscle was then subjected to an eccentric contraction (ECC) protocol consisting of 8 eccentric contractions (ECCs) at 3-minute intervals. A fiber length (L_f)-to-L_0 ratio of 0.45 was used to calculate L_f. Each ECC consisted of an initial 100 millisecond isometric contraction at optimal frequency immediately followed by a stretch of L_o to 30% of L_f beyond L_o at a velocity of 1 L_f/s at optimal frequency. The muscle was then passively returned to L_o at the same velocity. At 3, 15, 30, 45, and 60 minutes after the ECC protocol, isometric tetanic force was measured. After the analysis of the contractile properties, the muscle was weighed. The cross-sectional area (CSA) of muscle was determined by dividing the muscle mass by the product of L_f and the density of mammalian skeletal muscle (1.06 g/cm^3). The specific force was determined by dividing F_o by the CSA (kN/mm^2). 18-20 week-old male mice were used, and right and left EDL muscles from each mouse were employed whenever possible, with n=5 to 8 muscles used for each analysis. Each data point represents an individual EDL. Statistics were calculated using GraphPad Prism 8 software and Student's unpaired T-Test was used (two-sided). Differences were considered significant at a p-value less than 0.05.

H&E and Immunofluorescence Analysis of Skeletal Muscle

Histology and immunofluorescence of mouse skeletal muscle were performed as described previously **(*Goddeeris et al., 2013*)**. Mice were euthanized by cervical dislocation and directly after sacrifice, quadriceps muscles were isolated, embedded in OCT compound and then snap frozen in liquid nitrogen cooled 2-methylbutane. 10 µM sections were cut with a cryostat (Leica CM3050S Research Cryostat; Amsterdam, the Netherlands) and H&E stained using conventional methods. Whole digital images of H&E-stained sections were taken by a VS120-S5-FL Olympus slide scanner microscope (Olympus Corporation, Tokyo, Japan). For immunofluorescence analyses, a mouse monoclonal antibody to glycoepitopes on the sugar chain of α-DG (IIH6, 1:100 dilution, Developmental Studies Hybridoma Bank, University of Iowa; RRID: AB_2617216) was added to sections overnight at 4°C followed by Alexa Fluor®-conjugated goat IgG against mouse IgM (Invitrogen, Carlsbad, CA, 1:500 dilution), for 40 minutes. The sections were also stained with rabbit polyclonal antibody to β-DG (AP83; 1:50 dilution) followed by Alexa Fluor®-conjugated 488 Goat anti-rabbit IgG (1:500). Whole sections were imaged with a VS120-S5-FL Olympus slide scanner microscope. Antibody IIH6 is a monoclonal to the glycoepitope of α-DG **(*Ervasti et al., 1991*)**, and AP83 is a polyclonal antibody to the c-terminus of β-DG **(*Ervasti et al., 1991*)**, both of which have been described previously.

For histologic analysis of human skeletal muscle, H&E staining on 10 µm frozen section was performed using the Leica ST5020 Multistainer workstation (Leica Biosystems, Buffalo Grove, IL) according manufacturer's instructions. For immunofluorescence analysis, unfixed frozen serial sections (7 µm) were incubated with primary antibodies for 1 hour, and then with the appropriate biotinylated secondary antibodies for 30 minutes followed by streptavidin conjugated to Alexa Fluor 594 (ThermoFisher Scientific, UK) for 15 minutes. Primary antibodies used were mouse

monoclonal: α-DG IIH6 (clone IIH6C4) (***Ervasti et al., 1991***), β-DG (Leica, Milton Keynes, UK; clone 43DAG1/8D5). All washes were made in PBS and incubations were performed at room temperature. Sections were evaluated with a Leica DMR microscope interfaced to MetaMorph (Molecular Devices, Sunnyvale, CA).

Tissue Biochemical Analysis

30 slices of 30 µM thickness were taken with a with a cryostat (Leica CM3050S Research Cryostat) from skeletal muscle or heart that had been frozen in liquid nitrogen-cooled 2-methylbutane. For biochemical analysis of murine skeletal muscle, quadriceps muscle were used. Samples were solubilized in 500 µL of 1% Triton X-100 in 50 mM Tris pH 7.6 and 150 mM NaCl with protease inhibitors (per 10 mL buffer: 67 µL each of 0.2 M Phenylmethylsulfonylfluoride (PMSF), 0.1 M Benzamidine and 5 µL of each of Leupeptin (Sigma/Millipore) 5 mg/mL, Pepstatin A (Millipore) 1 mg/mL in methanol, Aprotinin (Sigma-Aldrich) 5 mg/mL, Calpeptin (Fisher/EMD Millipore) 1.92 mg/mL in Dimethyl Sulfoxide (DMSO), Calpain Inhibitor 1 (Sigma-Aldrich) 1.92 mg/mL in DMSO). Samples were vortexed for 4 minutes and solubilized for 2.5 hours at 4°C with rotation. Samples were then spun down at 12,000 rpm for 30 minutes at 4°C on a Beckman Tabletop Centrifuge. The supernatant was incubated with 100 µL WGA-Agarose slurry (Vector Biolabs, Malvern, PA, AL-1023) overnight at 4°C with rotation. The next day samples were washed three times in 50 mM Tris pH 7.6 and 150 mM NaCl with 0.1% TX-100 and protease inhibitors. 100 µL of 5X Laemmli Sample Buffer (LSB) was added, samples boiled for 10 minutes, and 125 µL of this was loaded in each lane of gels for western blotting.

Fibroblast Growth and Flow Cytometry

Fibroblasts used for biochemical analyses were grown in 20% Fetal Bovine Serum (FBS, Life Technologies, Carlsbad, CA) and 1% penicillin/streptomycin (Invitrogen). Cells were split at 1:2 every 2 days using Trypsin-EDTA (ThermoFisher Scientific, Waltham, MA).

For flow cytometry analyses, fibroblasts cultured from skin biopsies were grown in Dulbecco's modified Eagles medium (Invitrogen) with 20% fetal bovine serum (FBS, Life Technologies), 1% glutamax (Thermo Fisher Scientific) and 1% penicillin/streptomycin (Sigma-Aldrich). Upon approximately 90% confluence, cells were washed with PBS without Ca and Mg, detached with non-enzymatic dissociation solution (Sigma-Aldrich cat. C5914) and fixed in 2% paraformaldehyde for 10 minutes. Cells were subsequently incubated on ice with the following antibodies diluted in PBS/0.1% FBS: anti-α-DG IIH6 (Millipore) for 30 minutes, anti-mouse biotinylated IgM (Vector Labs, Burlingame, CA) for 20 minutes, Streptavidin-Phycoerythrin (BD Pharmingen) for 15 minutes. Negative controls for each fibroblast population were incubated with 0.1% FBS/PBS without the primary antibodies. Cells were washed twice and centrifuged at 1850g for 4 minutes, after each incubation step. After the last wash, cell pellets were re-suspended in 500 µL of PBS. A total of 10,000 event were acquired using the Cyan ADP analyser (Beckman Coulter, Brea, CA) and analysed using FlowJo software version 7.6.5 (Tree Star, USA).

Generation and Characterization of HAP1 Mutant Cell Lines

HAP1 cells (RRID: CVCL_Y019) are a haploid human cell line with an adherent, fibroblast-like morphology, originally derived from parent cell line KBM-7 (RRID: CVCL_A426). Wild-type C631 (a diploid cell line containing duplicated chromosomes of HAP1) were purchased from Horizon Discovery and gene-specific knockout HAP1 cells were generated by Horizon Discovery.

POMK knockout (KO) HAP1: HAP1 cells bearing a 10 bp deletion of exon 4 of the *POMK*, generated using the CRISPR/Cas9 system, were purchased from Horizon Discovery (HZGHC001338c004, clone 1338–4) and were previously described **(*Zhu et al., 2016*)**. *POMK* knockout (KO) HAP1 cells lack the single copy of the wild-type *POMK* allele and are therefore null at the *POMK* locus. The sequence of the guide RNA used is TGAGACAGCTGAAGCGTGTT. Absence of the wild-type *POMK* allele was confirmed by Horizon Discovery via PCR amplification and Sanger sequencing. PCR primers used for DNA sequencing are *POMK* Forward 5'-ACTTCTTCATCGCTCCTCGACAA-3', and *POMK* Backward 5'- GGATGCCACACTGCTTCCCTAA-3'. The identity of the cells has been authenticated by the company using the STR profiling method. Mycoplasma testing of the cells were performed on a routine basis to ensure the cells are not contaminated.

POMK/DG KO HAP1: HAP1 cells lacking both *POMK* and *DAG1* expression (*POMK/DG* KO HAP1 cells) were generated using CRISPR/Cas9 by Horizon Discovery. A 16 bp deletion in the DAG1 gene (exon 2) was introduced into the *POMK* KO HAP1 line (HZGHC001338c004). The sequence of the Guide RNA is CCGACGACAGCCGTGCCATC; NM_004393. PCR primers for DNA sequencing were forward TAGCAAGACTATCGACTTGAGCAAA and reverse GCAATCAAATCTGTTGGAATGGTCA.

POMK/LARGE KO HAP1: HAP1 cells lacking both *POMK* and *LARGE* expression (*POMK/LARGE* KO HAP1 cells) (HZGHC007364c011) were generated using CRISPR/Cas9 by Horizon Discovery. A 43 bp deletion of exon 3 of LARGE was introduced into the *POMK* KO HAP1 line (HZGHC001338c004). The guide RNA sequence was CTCGGCGATGGGATGGGGCT and the primer sequence was PCR forward

GAGGCATGGTTCATCCAGATTAAAG and PCR reverse CTTTACCTCGCATTTCTCCACGA.

POMK/ISPD KO HAP1: HAP1 cells containing a 1 bp insertion of exon 4 of the *POMK* gene, generated using the CRISPR/Cas9 system, were purchased from Horizon Discovery (HZGHC001338c001, clone 1338–1). The mutation in *POMK* is predicted to lead to a frameshift. These cells also lacked expression of *ISPD*. The Guide RNA sequence was TGAGACAGCTGAAGCGTGTT. The sequences of PCR primers were PCR forward ACTTCTTCATCGCTCCTCGACAA and PCR reverse GGATGCCACACTGCTTCCCTAA.

LARGE KO HAP1: HAP1 cells (clone 122-6, HZGHC000122c006) were purchased from Horizon Discovery. Cells were generated using a CRISPR/Cas9-mediated 1 bp deletion of exon 3. The guide RNA sequence was GCTCTCGCGCTCCCGCTGGC and the primer sequence for 122-7 was PCR forward ATGGAGTAGGTCTTGGAGTGGTT and PCR reverse GAGGCATGGTTCATCCAGAGTTAAAG.

FKTN KO HAP1: HAP1 cells (clone 721-10, catalog number 32597-10) were purchased from Horizon Discovery. CRISPR/Cas9 was used to introduce 16 bp deletion of exon 3. The sequence of the guide RNA was CAGAACTTGTCAGCGTTAAA and the sequences of PCR forward CAGATCAAAGAATGCCTGTGGAAAT and PCR reverse TGCAAAGAGAAGTGTGATCAGAAAA.

<u>Adenovirus Production</u>

DGE (Delta H30- A316) was generated and described previously **(*Hara et al., 2011; Kanagawa et al., 2004; Kunz et al., 2001*)**. DG T317A, DG T319A, and DG T317A/T319A were first subcloned into an Fc-tagged DG construct (DGFc3) **(*Hara et al., 2011; Kanagawa et al., 2004; Kunz et al., 2001*)**. The *KpnI-XhoI* fragments from the DGFc3 mutants corresponding to the mutant

constructs (DG T317A, DG T319A, or DG T317A/T319A) were then subcloned into pAd5RSVK-NpA (obtained from the University of Iowa Viral Vector Core) as was the *XhoI-XbaI* fragment from an adenovirus encoding dystroglycan-WT. *E1*-deficient recombinant adenoviruses (Ad5 RSV DG-WT, DG T317/T319, DG T317A, DG T319A, DGE, Ad-*POMK* WT) were generated by the University of Iowa Viral Vector Core (VVC) using the RAPAd system **(*Anderson et al., 2000*)**. Assays for replication competence of adenoviruses were performed to check for contamination. Ad-*POMK*-WT and Ad-*POMK*-D204A were generated by ViraQuest Inc. (North Liberty, IA) using the RAPAd system and was described previously **(*Zhu et al., 2016*)**. Ad-*POMK*-D204N was also generated by ViraQuest Inc. Absence of the viral *E1* DNA sequence was confirmed by ViraQuest Inc. after PCR amplification of the viral DNA and staining on DNA agarose gel electrophoresis. Replication competence of adenoviruses was negative as assessed by plaque forming assays in cells performed from 10^9 viral particles up to 14 days. Adenoviral *Fukutin* (*FKTN*) and *Isoprenoid Synthase Domain-Containing* (*ISPD*) have been described previously **(*Hara et al., 2011*)**. Adenoviral *LARGE* has been described previously **(*Barresi et al., 2004*)**.

DGFc340TEV was cloned into the pUC57-mini vector by GenScript **(*Hara et al., 2011; Kanagawa et al., 2004; Kunz et al., 2001*)**. The insert includes TEV protein cleavage site between amino acids (AAs) 1-340 of rabbit DG and human IgG1 Fc. The insert was subcloned in pcDNA3 expression vector with *EcoRI*. Subsequently, FseI-x-340 AAs DG-TEV-6xHis-*NotI* fragment was obtained using pcDNA3DGFc340TEV as a PCR template. *FseI*-x-340 AAs DG-TEV-6xHis-*NotI* was ligated into pcDNA3DGFc340TEV digested with *FseI* and *NotI* to construct DG340TEVHis, which includes 1-340 AAs of rabbit DG, TEV site, and 6x Histidine. The construct was also inserted in pacAd shuttle plasmid from the VVC to generate the adenoviral vector. Next, *FseI*-x-390 AAs-TEV-6xHis-*NotI* was obtained using pcDNA3rbtDG as a PCR template and ligated into

the pcDNA3DG340TEVHis digested with *FseI* and *NotI* to construct DG390TEVHis, which includes 1-390 AAs of rabbit DG, TEV site, and 6x Histidine. The construct was also inserted in pacAd shuttle plasmid from the VVC to generate the Ad virus vector. E1-deficient recombinant adenoviruses were generated by the University of Iowa Viral Vector Core using the RAPAd system **(*Kunz et al., 2001*)**.

HAP1 Cell Culture and Adenovirus Infection

HAP1 cells were maintained at 37°C and 5% CO_2 in Iscove's Modified Dulbecco's Medium (IMDM, Gibco) supplemented with 10% Fetal Bovine Serum (FBS) and 1% penicillin/streptomycin (Invitrogen). Cells were split every 3 days at 1:10 using Trypsin-EDTA (ThermoFisher Scientific). On day 1, media was changed to 2% IMDM, and an average of 5.9×10^6 *POMK* KO HAP1 cells were infected at the indicated multiplicity of infection (MOI) of the indicated adenovirus. On day 2, infection medium was replaced with 10% IMDM, and on day three the cells were processed for biochemical analyses.

Glycoprotein Isolation and Biochemical Analyses from Cultured Cells

For western blots and laminin overlay, HAP1 cells and fibroblasts were washed twice in ice-cold Dulbecco's Phosphate-Buffered Saline (DPBS, Gibco). The second PBS wash contained the protease inhibitors (0.23 mM PMSF and 0.64 mM Benzamidine). Plates were scraped, spun down for 5 minutes at 14, 000 rpm at 4ºC, and pellets were solubilized in 1% Triton X-100 in Tris-buffered saline (TBS, 50 mM Tris-HCl pH 7.6, 150 mM NaCl) with protease inhibitors (0.23 mM PMSF and 0.64 mM Benzamidine) for 1 hour at 4ºC. Samples were then spun down at 14,000 rpm for 5 minutes, and supernatants incubated in 200 µL wheat-germ agglutinin (WGA)-agarose (Vector Laboratories, AL-1023) as previously described **(*Michele et al., 2002; Goddeeris et al., 2013*)**. The following day, WGA beads were washed three times with 0.1% Triton X-100-TBS

plus protease inhibitors and heated to 99°C for 10 minutes with 250 µL of 5X Laemmli sample buffer. Samples were run on SDS-PAGE and transferred to PVDF-FL membranes (Millipore) as previously published **(*Michele et al., 2002; Goddeeris et al., 2013*)**.

Immunoblotting and Ligand Overlay

The mouse monoclonal antibody against α-DG (IIH6, Developmental Studies Hybridoma Bank, University of Iowa; RRID: AB_2617216) was characterized previously and used at 1:100 **(*Ervasti et al., 1991*)**. The polyclonal antibody, AF6868 (R&D Systems, Minneapolis, MN; RRID: AB_10891298), was used at a concentration of 1:200 for immunoblotting the core α-DG and β-DG proteins, and the secondary was a Donkey anti-Sheep (LI-COR Bioscience, Lincoln, NE) used at 1:2000 concentration. Anti-POMK (Novus Biologicals, Littleton, CO, 6f10) was used at 1:500, and the secondary was 1:2000 Goat anti-Mouse IgG1 (LI-COR Bioscience). The antibody against the Na/K ATPase (BD Biosciences, San Jose, CA, 610993) was used at 1:1000 in 5%-milk Blotto, and the secondary was 1:10,000 Goat anti-Mouse IgG1 (LI-COR Bioscience). Anti-myc (Millipore Sigma, Clone 4A6) was used at 1:2,000 in 2% milk and the secondary was 1:2,000 Goat anti-Mouse IgG1 (LI-COR Bioscience). Blots were developed with infrared (IR) dye-conjugated secondary antibodies (LI-COR Bioscience) and scanned using the Odyssey infrared imaging system (LI-COR Bioscience). Blot images were captured using the included Odyssey image-analysis software.

Laminin overlay assays were performed as previously described **(*Michele et al., 2002; Goddeeris et al., 2013*)**. PVDF-FL membranes were blocked in laminin binding buffer (LBB: 10 mM triethanolamine, 140 mM NaCl, 1 mM $MgCl_2$, 1 mM $CaCl_2$, pH 7.6) containing 5% milk followed by incubation with mouse Engelbreth-Holm-Swarm (EHS) laminin (ThermoFisher, 23017015) overnight at a concentration of 7.5 nM at 4°C in LBB containing 3% bovine serum albumin (BSA)

and 2 mM $CaCl_2$. Membranes were washed and incubated with anti-laminin antibody (L9393; Sigma-Aldrich 1:1000 dilution) followed by IRDye 800 CW dye-conjugated donkey anti-rabbit IgG (LI-COR, 926-32213) at 1:2500 dilution.

EDTA Treatment of Ligand Overlays

EDTA treatment of laminin overlay assays were performed as described above for laminin overlays; however, calcium was excluded from all buffers made with LBB (i.e. 5% milk-LBB, 3% BSA-LBB) and 10 mM EDTA was added to all LBB-based buffers, including LBB wash buffer, 5% milk-LBB, and 3% BSA-LBB buffers.

POMK Assay

HAP1 cells were washed twice in ice-cold PBS, scraped, and spun down at 14,000 rpm for 5 minutes at 4°C. After removing supernatant, the cell pellet was resuspended in 0.1 M MES buffer pH 6.5 with 1% Triton X-100 with Protease Inhibitors (0.23 mM PMSF and 0.64 mM Benzamidine) for 1 hour at 4°C rotating. Samples were spun down again, and the supernatant was incubated with 200 µL of WGA-agarose beads (Vector Biolabs, AL-1023) overnight at 4°C with rotation. Samples were washed the next day three times in 0.1 M MES pH 6.5 with 0.1% Triton X-100 and protease inhibitors, and 100 µL of the beads were resuspended in 100 µL of the wash buffer.

For fibroblast POMK activity measurements, cells were processed as above and solubilized in 1% TX-100 in 50 mM Tris and 150 mM NaCl pH 7.6 with protease inhibitors as described above and incubated with WGA-agarose beads. The next day, WGA beads were washed three times and resuspended in 0.1% TX-100 in 0.1 M MES pH 6.5 buffer with protease inhibitors.

For measurement of mouse and human skeletal muscle POMK activity, 30 slices of 30 µM thickness were taken using a Leica 3050s cryostat from quadriceps muscle frozen in liquid

nitrogen-cooled 2-methylbutane. Samples were solubilized in 250 µL of 1% Triton X-100 in 0.1 M MES pH 6.5 with protease inhibitors (per 10 mL buffer: 67 µL each of 0.2 M PMSF, 0.1 M Benzamidine and 5 µL/10 mL of buffer of Leupeptin (Sigma/Millipore) 5 mg/mL, Pepstatin A (Millipore) 1 mg/mL in methanol, Aprotinin (Sigma-Aldrich) 5 mg/mL, Calpeptin (Fisher/EMD Millipore) 1.92 mg/mL in Dimethyl Sulfoxide (DMSO), Calpain Inhibitor 1 (Sigma-Aldrich) 1.92 mg/mL in DMSO). Samples were solubilized for 2.5 hours at 4°C on a rotator. Samples were then spun down at 14, 000 rpm for 30 minutes at 4°C on a Beckman Tabletop Centrifuge. The supernatant (total lysate) was separated from the pellet, and 10 µL of this was used for POMK assays.

For POMK reaction in HAP1 cells and fibroblasts, 20 µL slurry (consisting of 10 µL beads and 10 µL MES buffer) was incubated with reaction buffer for a final reaction volume of 40 µL. For POMK assay from skeletal muscle, 10 µL of total lysate was incubated with 20 µL of reaction buffer for a reaction volume of 30 µL. The final reaction concentration was 10 mM ATP, 10 mM MnCl2, 10 mM MgCl2, 10 µM GGM-MU, 0.1% TX-100 in 0.1 M MES Buffer pH 6.5. Reactions were run at 37°C for 24 hours for HAP cells, 48 hours for fibroblasts, or 16 hours for skeletal muscle. Experiments were done in triplicate, with each replicate representing a separate plate of cells or animal. After POMK reaction, 6 µL 0.5 M EDTA was added to 30 µL of reaction supernatant, and the mixture boiled for 5 minutes. 25 µL of this mixture and added to 30 µL ddH20 in HPLC vial and run on an LC18 column of a reverse-phase HPLC (Shimadzu Scientific, Columbia, Maryland) with a 16% B med sensitivity gradient. The reaction was analyzed using a 4.6 x 250 mm Supelcosil LC-18 column (Supelco). Solvent A was 50 mM ammonium formate (pH 4.0), and solvent B was 80% acetonitrile in solvent A. Elution of the MU derivative was monitored by fluorescence detection (325 nm for excitation, and 380 nm for emission) and peak

area used as a measure of activity. The enzymatic activity was calculated as the peak area of the product.

B4GAT1 Assay

For the assessment of endogenous B4GAT1 activity in skeletal muscle, Triton X-100-solubilized lysates (10 µl for human skeletal muscle or 40 µL for mouse skeletal muscle) were incubated in a volume of 50 µL (human skeletal muscle) for 12 hours at 37°C, with 0.4 mM Xylose-β-MU (Xyl-β-MU) and 10 mM Uridine diphosphate glucuronic acid (UDP-GlcA) in 0.1 M MES buffer, pH 6.0, at 5 mM $MnCl_2$, 5 mM $MgCl_2$, and 0.05% Triton X-100 **(*Willer et al., 2014*)**. The reaction was terminated by adding 25 µL of 0.1 M EDTA and boiling for 5 minutes, and the supernatant was analyzed using an LC-18 column. Both the substrate Xyl-β-MU and the product GlcA-Xyl-β-MU were separated on a 16% acetonitrile isocratic gradient. Elution of the MU derivative product was monitored by fluorescence detection (325 nm for excitation, and 380 nm for emission). The percent conversion of substrate to product was used as the activity of the B4GAT1 in the 10 µL sample. The B4GAT1 activity then was normalized against the amount of protein measured in the 10 µL of sample using the DC Protein Assay (Bio-Rad, Hercules, CA) with BSA as the standard. For assessment of B4GAT1 activity in HAP cells, the HAP WGA beads were incubated in a volume of 80 µL for 26 h at 37°C, with 0.4 mM Xyl-β-MU and 10 mM UDP-GlcA in 0.1 M MES buffer, pH 6.0, at 5 mM $MnCl_2$, 5 mM $MgCl_2$, and 0.05% Triton X-100. The reaction was terminated by adding 25 µL of 0.1 M EDTA and boiling for 5 minutes, and the supernatant was analyzed using an LC-18 column. Elution of the MU derivative was monitored by fluorescence detection (325 nm for excitation, and 380 nm for emission) and peak area used as a measure of activity. The percent product was determined by taking the product peak area and dividing by the

total peak areas of substrate plus product peak. Then this number was taken and multiplied by 100 for percent conversion to product.

LARGE Assay

For the assessment of endogenous LARGE GlcA-T activity in skeletal muscle, Triton X-100-solubilized lysates were incubated in a volume of 25 µL for 3 h at 37°C, with 0.4 mM Xyl-α1,3-GlcA-β-MU and 10 mM UDP-GlcA in 0.1 M MES buffer, pH 6.0, at 5 mM $MnCl_2$, 5 mM $MgCl_2$, and 0.5% Triton X-100. The reaction was terminated by adding 25 µL of 0.1 M EDTA and boiling for 5 minutes, and the supernatant was analyzed using an LC-18 column. Elution of the MU derivative was monitored by fluorescence detection (325 nm for excitation, and 380 nm for emission) and peak area used as a measure of activity. The GlcA-T activity was assessed by subtracting the background observed in the negative control sample without donor sugar and normalized against the amount of protein measured using the DC Protein Assay (Bio-Rad).

For assessment of LARGE enzymatic activity in HAP cells, the Triton X-100 solubilized HAP cells were loaded onto WGA beads and processed as described for POMK assay above. The next day after wash, beads were incubated in a volume of 90 µL with 0.4 mM Xyl-α1,3-GlcA-β-MU and 10 mM UDP-GlcA in 0.1 M MOPS buffer, pH 6.0, at 5 mM $MnCl_2$, 5 mM $MgCl_2$, and 0.05% Triton X-100. The samples were run for 46 h at 37°C. The reaction was terminated by adding 25 µL of 0.25 M EDTA and boiling for 5 minutes, and the supernatant was analyzed using an LC-18 column.

For the assessment of endogenous LARGE activity in fibroblasts, supernatants from Triton X-100 solubilized fibroblasts were (20 µL) directly used. Supernatants were incubated in a volume of 100 µL for 24 h at 37°C, with 0.4 mM Xyl-α1,3-GlcA-β-MU and 10 mM UDP-GlcA in 0.1 M MES buffer, pH 6.0, at 5 mM MnCl2, 5 mM MgCl2, and 0.5% Triton X-100. The reaction was

terminated by adding 25 µL of 0.1 M EDTA and boiling for 5 minutes, and the supernatant was analyzed using an LC-18 column.

Elution of the MU derivative was monitored by fluorescence detection (325 nm for excitation, and 380 nm for emission) and peak area used as a measure of activity. The percent product was determined by taking the product peak area and dividing by the total peak areas of substrate plus product peak. Then this number was taken and multiplied by 100 for percent conversion to product.

B3GALNT2 Assay

To assess B3GALNT2 activity in HAP1 cells, 20 µL of the WGA beads from HAP1 cells were incubated with a 20 µL volume of the reaction mix. The final volume of reaction buffer was 40 µL (30 µL reaction mixture and 10 µL WGA-beads). The final concentrations were 10 mM $MgCl_2$, 10 mM $MnCl_2$, 0.1 M MES pH 6.5, 10 µM GGM-MU, and 10 mM UDP-GlcNac. Reactions were run at 37°C for 72 hours. Experiments were done in triplicate, with each replicate representing a separate plate of cells. After B3GALNT2 reaction, 6 µL 0.5 M EDTA was added to 30 µL of reaction supernatant, and the mixture boiled for 5 minutes. 25 µL of this mixture and added to 30 µL ddH20 in HPLC vial and run on an LC18 column of a reverse-phase HPLC (Shimadzu Scientific) with a 16% B med sensitivity gradient. The reaction was analyzed using a 4.6 x 250 mm Supelcosil LC-18 column (Supelco, Bellefonte, PA). Solvent A was 50 mM ammonium formate (pH 4.0), and solvent B was 80% acetonitrile in solvent A. Elution of the MU derivative was monitored by fluorescence detection (325 nm for excitation, and 380 nm for emission) and peak area used as a measure of activity. The enzymatic activity was calculated as the peak area of the product.

Digestion of α-DG with Exoglycosidases

Exoglycosidase treatment was carried out as described previously **(*Briggs et al., 2016; Salleh et al., 2006; Moracci et al., 2000*)**. *T. maritima* β-glucuronidase **(*Salleh et al., 2006; Moracci et al., 2000*)** (Bgus) and *S. solfataricus* α-xylosidase (Xylsa), both bearing a His-tag were overexpressed in *E. coli*, and purified using TALON metal affinity resin as described and activity determined as described **(*Salleh et al., 2006; Moracci et al., 2000*)** with some modifications. Briefly, the cell pellet was resuspended in 20 mM HEPES buffer (pH 7.3), 150 mM NaCl, 0.1% NP-40 and sonicated. After centrifugation (30 minutes at 40,000 x *g*), the crude extract was incubated with Benzonase (Novagen) for 1 hour at room temperature and then heat-fractionated for 10 minutes at 75°C. The supernatant was purified by using Talon metal affinity resin.

Samples to be digested by Bgus and Xylsa were exchanged into 150 mM sodium acetate (pH 5.5) solution and mixed with Bgus (0.45 U) and/or Xylsa (0.09 U), or no enzymes, and incubated overnight at 65°C. Samples were then run on SDS-PAGE, transferred to PVDF-FL (Millipore), and probed with anti-α-DG core antibody (AF6868) and anti-α-DG glycan antibody (IIH6). Enriched rabbit α-DG (100 μL of the 150 mM sodium acetate (pH 5.5) solution) was mixed with Bgus (0.45 U) and/or Xylsa (0.09 U), or no enzymes, and incubated overnight at 65°C. Samples were then run on SDS-PAGE, transferred to PVDF-FL (Millipore), and subjected to immunoblotting.

Solid Phase Assay

Solid phase assays were performed as described previously **(*Michele et al., 2002; Goddeeris et al., 2013*)**. Briefly, WGA eluates were diluted 1:50 in TBS and coated on polystyrene ELISA microplates (Costar 3590) overnight at 4°C. Plates were washed in LBB and blocked for 2 hours in 3% BSA/LBB at RT. The wells were washed with 1% BSA/LBB and incubated for 1 hour with

L9393 (1:5,000 dilution) in 3% BSA/LBB followed by incubation with Horseradish Peroxidase (HRP)-conjugated anti-rabbit IgG (Invitrogen, 1:5,000 dilution) in 3% BSA/LBB for 30 minutes. Plates were developed with o-phenylenediamine dihydrochloride and H_2O_2, and reactions were stopped with 2 N H_2SO_4. Absorbance per well was read at 490 nm by a microplate reader.

Statistics

The included Shimadzu post-run software was used to analyze POMK, LARGE, and B4GAT1 activity in fibroblasts and mouse skeletal muscle, and the percent conversion to product was recorded. The means of three experimental replicates (biological replicates, where each replicate represents a different pair of tissue culture plates or animals, i.e. control and knockout) were calculated using Microsoft Excel, and the mean percent conversion to product for the WT or control sample (Control human fibroblasts or $POMK^{LoxP/LoxP}$ skeletal muscle, respectively) reaction was set to 1. Percent conversion of each experimental reaction was subsequently normalized to that of the control, and statistics on normalized values were performed using GraphPad Prism 8. For analysis of POMK and LARGE activity in fibroblasts and mouse skeletal muscle, Student's T-Test was used (two-sided). Differences were considered significant at a p-value less than 0.05. Graph images were also created using GraphPad Prism and the data in the present study are shown as the means +/- SD unless otherwise indicated. The number of sampled units, n, upon which we report statistics for *in vivo* data, is the single mouse (one mouse is n=1). For measure of POMK activity in HAP1 cells, the percent conversion from GGM-MU to GGM(P)-MU was first calculated using the included Shimadzu analysis software. The means plus standard deviations of the percent conversion to GGM(P)-MU for three experimental replicates was calculated using GraphPad Prism 8. One-way ANOVA with the Dunnett's Method for Multiple Comparisons was performed, and the data for the *POMK* KO HAP1 sample set as the control.

Differences were considered significant at a p-value less than 0.05. Graph images were created in GraphPad and show mean +/- SD.

To measure POMK activity in control and NH13-284 skeletal muscle, we only performed one experimental replicate due to the limited amount of sample available. To measure B4GAT1 activity, two technical replicates were performed from skeletal muscle. Protein concentration from control and NH13-284 skeletal muscle was also measured using two technical replicates. The percent conversion to product for the B4GAT1 reaction was divided by the protein concentration, and the values for these two technical replicates graphed using GraphPad Prism 8. The graph reported is shown as the mean +/- SD.

For flow cytometry analyses, six experimental replicates were performed, and the mean fluorescence intensity (MFI) reported. Statistics were performed using the Student's unpaired T-test, two-sided in GraphPad Prism 8 and the values reported as mean +/- SD.

NMR Spectroscopy

1D ^{1}H NMR spectra of the core M3 trisaccharides GGM-MU and GGMp-MU in the absence and presence of POMK or LARGE were acquired at 25°C on a Bruker Avance II 800 MHz NMR spectrometer equipped with a sensitive cryoprobe by using a 50 ms T_2 filter consisting of a train of spin-lock pulses to eliminate the broad resonances from the protein **(*Mayer at al., 2001*)**. *Danio rerio* POMK titrations were performed in 25 mM Tris (pH 8.0), 180 mM NaCl, and 10 mM $MgCl_2$ in 98% D_2O. LARGE titrations were performed in 20 mM HEPES, 150 mM NaCl, pH 7.3 in 90% H_2O/10% D_2O. The ^{13}C and ^{1}H resonances of the trisaccharides were reported previously **(*Yoshida-Moriguchi et al., 2010*)**. The ^{1}H chemical shifts are referenced to 2,2-dimethyl-2-silapentane-5-sulfonate. The NMR spectra were processed using NMRPipe **(*Delaglio et al., 1995*)** and analyzed using NMRView **(*Johnson et al., 1994*)**. The glycan binding affinity to POMK and

LARGE was determined using glycan-observed NMR experiments as described previously (***Briggs et al., 2016***). For the resolved anomeric trisaccharide peak, the bound fraction was calculated by measuring the difference in the peak intensity in the absence (free form) and presence (bound form) of POMK or LARGE, and then dividing by the peak intensity of the free form. To obtain dissociation constant, the data were fitted to the standard quadratic equation using GraphPad Prism (GraphPad Software). The standard deviation from data fitting is reported.

Mass Spectrometry

In order to generate DG fusion proteins for MS analyses, HAP cells were grown in IMDM with 10% FBS and 1% penicillin/streptomycin on p150 plates. When plates were 80% confluent, cells were washed twice with DPBS, media changed to serum-free IMDM with 1% penicillin/streptomycin (Invitrogen), and cells infected at high MOI (250-1000) of adenovirus expressing DG390TEVHis. Three days later, the media was harvested and stored at 4 degrees Celsius until samples were ready for MS analysis.

Reductive elimination. Glycans were reductively eliminated from DG390 proteins and purified on a 50WS8 Dowex column, and the purified glycans were subjected to permethylation and purified according to published methods (***Jang-Lee et al., 2006; Zhang et al., 2014***). Briefly, the freeze-dried DG390 sample was dissolved in 55 mg/mL potassium borohydride in 1 mL of a 0.1 M potassium hydroxide solution. The mixture was incubated for 18 hours at 45°C and quenched by adding five to six drops of acetic acid. The sample was loaded on the Dowex column and subsequently eluted with 5% acetic acid. The collected solution was concentrated and lyophilized, and excessive borates were removed with 10% methanolic acetic acid.

Permethylation. For the permethylation reaction, three to five pellets per sample of sodium hydroxide were crushed in 3 mL dry dimethyl sulfoxide. Methyl Iodine (500 mL) as well as the

resulting slurry (0.75 mL) were added to the sample. The mixture was agitated for 15 minutes and quenched by adding 2 mL ultrapure water with shaking. The glycans were extracted with chloroform (2 mL) and washed twice with ultrapure water. Chloroform was removed under a stream of nitrogen. The permethylated glycans were loaded on a C18 Sep-pak column, washed with 5 mL ultrapure water and successively eluted with 3 mL each of 15, 35, 50 and 75% aq. acetonitrile. The solutions were collected and lyophilized.

Mass spectrometry. A Bruker Autoflex III MALDI TOF/TOF was used for acquisition of all MALDI MS data. An in-house made BSA digest was used to calibrate the MS mode. 3,4-diaminobenzophenone was used as the matrix. Permethylated samples were dissolved in 10 mL of methanol, and 1 µL of this solution was premixed with 1 µL matrix. 1 µL of this mixture was spotted on the plate.

Data Availability

All data generated or analyzed during this study are included in this published article.

Acknowledgements

The BRC/ MRC Centre for Neuromuscular Diseases Biobank is acknowledged for providing patients' serum and biopsy samples. The Muscular Dystrophy UK support to the GOSH Neuromuscular Centre is also gratefully acknowledged. We wish to thank Norma Sinclair, Patricia Yarolem, JoAnn Schwarting and Rongbin Guan for their technical expertise in generating transgenic mice.

Authors' Contributions

ASW and KPC designed experiments and wrote the manuscript. ASW, HO, SJ, TY, TY, DV, JMH, MC, ST, MEA, LY, MD, SOL, and SJP performed experiments. AM, ST, JX, JED, and FM provided critical information and materials regarding the patient. FM was involved in meaningful discussions regarding the manuscript. All authors contributed to and gave feedback on the manuscript.

Competing Interests

The authors declare no competing financial interests. Correspondence and requests for materials should be addressed to K.P.C. (kevin-campbell@uiowa.edu).

Funding

This work was supported in part by a Paul D. Wellstone Muscular Dystrophy Specialized Research Center grant (1U54NS053672 to KPC). S. T and F.M. are supported by the National Institute for Health Research Biomedical Research Centre at Great Ormond Street Hospital for Children NHS Foundation Trust and University College London. A.S.W. is a student in the

University of Iowa Medical Scientist Training Program, which is funded by Medical Scientist Training Program Grant by the National Institute of General Medical Sciences (NIGMS) 5 T32 GM007337. Transgenic mice were generated at the University of Iowa Genome Editing Core Facility directed by William Paradee, PhD and supported in part by grants from the NIH and from the Roy J. and Lucille A. Carver College of Medicine. KPC is an investigator of the Howard Hughes Medical Institute.

References

Anderson, R. D., Haskell, R. E., Xia, H., Roessler, B. J., & Davidson, B. L. A simple method for the rapid generation of recombinant adenovirus vectors. *Gene Ther.* **7**, 1034-1038 (2000). DOI: 10.1038/sj.gt.3301197, PMID: 10871752

Barresi, R., Michele, D.E., Kanagawa, M., Harper, H.A., Dovico, S.A., Satz, J.S., Moore, S.A., Zhang, W., Schachter, H., Dumanski, J.P., Cohn, R.D., Nishino, I., Campbell, K.P. LARGE can functionally bypass alpha-dystroglycan glycosylation defects in distinct congenital muscular dystrophies. *Nat Med.* **10**, 696-703 (2004). DOI: 10.1038/nm1059, PMID: 15184894

Briggs, D. C., Yoshida-Moriguchi, T., Zheng, T., Venzke, D., Anderson, M.E., Strazzulli, A., Moracci, M., Yu, L., Hohenester, E., Campbell, K.P. Structural basis of laminin binding to the LARGE glycans on dystroglycan. *Nat Chem Biol.* **12**, 810-814 (2016). DOI: 10.1038/nchembio.2146, PMID: 27526028

Brüning, J. C., Michael, M.D., Winnay, J.N., Hayashi, T., Hörsch, D., Accili, D., Goodyear, L.J., Kahn, C.R. A muscle-specific insulin receptor knockout exhibits features of the metabolic

syndrome of NIDDM without altering glucose tolerance. *Mol Cell.* ***5***, 559-569 (1998). DOI: 10.1016/s1097-2765(00)80155-0, PMID: 9844629

Cohn, R.D., Henry, M.D., Michele, D.E., Barresi, R., Saito, F., Moore, S.A., Flanagan, J.D., Skwarchuk, M.W., Robbins, M.E., Mendell, J.R., Williamson, R.A., Campbell, K.P. Disruption of DAG1 in differentiated skeletal muscle reveals a role for dystroglycan in muscle regeneration. *Cell*. **110**, 639-648 (2002). DOI: 10.1016/s0092-8674(02)00907-8, PMID: 12230980

Delaglio, F., Grzesiek, S., Vuister, G.W., Zhu, G., Pfeifer, J., Bax, A. NMRPipe: a multidimensional spectral processing system based on UNIX pipes. *J. Biomol. NMR.* **6**, 277-293 (1995). DOI: 10.1007/BF00197809, PMID: 8520220

Di Costanzo, S. Balasubramanian, A., Pond, H.L., Rozkalne, A., Pantaleoni, C., Saredi, S., Gupta, V.A., Sunu, C.M., Yu, T.W., Kang, P.B., Salih, M.A., Mora, M., Gussoni, E., Walsh, C.A., Manzini, M.C. POMK mutations disrupt muscle development leading to a spectrum of neuromuscular presentations. *Hum Mol Genet*. **23**, 5781-5792 (2014). DOI: 10.1093/hmg/ddu296, PMID: 24925318

Ervasti, J. M. & Campbell, K. P. Membrane organization of the dystrophin-glycoprotein complex. *Cell*. **66**, 1121-1131 (1991). DOI: 10.1016/0092-8674(91)90035-w, PMID: 1913804

Gerin, I., Ury, B., Breloy, I., Bouchet-Seraphin, C., Bolsée, J., Halbout, M., Graff, J., Vertommen, D., Muccioli, G.G., Seta, N., Cuisset, J.-M., Dabaj, I., Quijano-Roy, S., Grahn, A., Schaftingen, E.V., Bommer, G.T. ISPD produces CDP-ribitol used by FKTN and FKRP to transfer ribitol phosphate onto α-dystroglycan. *Nat. Commun.* **7**, 11534 (2016). DOI: 10.1038/ncomms11534, PMID: 27194101

Goddeeris, M. M., Wu, B., Venzke, D., Yoshida-Moriguchi, T., Saito, F., Matsumura, K., Moore, S.A., Campbell, K.P. LARGE glycans on dystroglycan function as a tunable matrix scaffold to prevent dystrophy. *Nature*. **503**, 136-140 (2013). DOI: 10.1038/nature12605, PMID: 24132234

Han, R., Kanagawa, M., Yoshida-Moriguchi, T., Rader, E.P., Ng, R.A., Michele, D.E., Muirhead, D.E., Kunz, S., Moore, S.A., Iannaccone, S.T., Miyake K., McNeil, P.L., Mayer, U., Oldstone, M.B.A., Faulkner, J.A., Campbell, K.P. Basal lamina strengthens cell membrane integrity via the laminin G domain-binding motif of α-dystroglycan. Proceedings of the National Academy of Sciences. **106**, 12573-12579 (2009). DOI: 10.1073/pnas.0906545106, PMID: 19633189

Hara, Y., Balci-Hayta, B., Yoshida-Moriguchi, T., Kanagawa, M., Beltrán-Valero de Bernabé., Gündeşli, H., Willer, T., Satz, J.S., Crawford, R.W., Burden, S.J., Kunz, S., Oldstone, M.B.A., Accardi, A., Talim, B., Muntoni, F., Topaloğlu, H., Dinçer, P., Campbell, K.P. A dystroglycan mutation associated with limb-girdle muscular dystrophy. *N Engl J Med.* **364**, 939-946 (2011). DOI: 10.1056/NEJMoa1006939, PMID: 21388311

Hara, Y., Kanagawa, M., Kunz, S., Yoshida-Moriguchi, T., Satz, J.S., Kobayashi, Y.M., Zhu, Z., Burden, S.J., Oldstone, M.B.A., Campbell, K.P. Like-acetylglucosaminyltransferase (LARGE)-dependent modification of dystroglycan at Thr-317/319 is required for laminin binding and arenavirus infection. *Proc Natl Acad Sci U S A.* **108**, 17426-17431 (2011). DOI: 10.1073/pnas.1114836108, PMID: 21987822

Hohenester, E. Laminin G-like domains: dystroglycan-specific lectins. *Current Opinion in Structural Biology*. **56**, 56-63 (2019). DOI: 10.1016/j.sbi.2018.11.007, PMID: 30530204

Hohenester, E., Tisi, D., Talts, J. F., & Timpl, R. The crystal structure of a laminin G-like module reveals the molecular basis of α-dystroglycan binding to laminins, perlecan, and agrin. *Mol Cell.* **4**, 783-792 (1999). DOI: 10.1016/s1097-2765(00)80388-3, PMID: 10619025

Hudson, BG. Tryggvason, K., Sundaramoorthy, M., Neilson, E.G. Alport's syndrome, Goodpasture's syndrome, and type IV collagen. *N Engl J Med.* **348**, 2543-2556 (2003). DOI: 10.1056/NEJMra022296, PMID: 12815141

Inamori, K., Yoshida-Moriguchi, T., Hara, Y., Anderson, M.E., Yu, L., Campbell, K.P. Dystroglycan function requires xylosyl- and glucuronyltransferase activities of LARGE. *Science*. **335**, 93-96 (2012). DOI: 10.1126/science.1214115, PMID: 22223806

Jae, L.T., Raaben, M., Riemersma, M., van Beusekom, E., Blomen, V.A., Velds, A., Kerkhoven, R.M., Carette, J.E., Topaloglu, H., Meinecke, P., Wessels, M.W., Lefeber, D.J., Whelan, S.P., van Bokhoven, H., Brummelkamp, T.R. Deciphering the glycosylome of dystroglycanopathies using haploid screens for lassa virus entry. *Science*. **340**, 479-483 (2013). DOI: 10.1126/science.1233675, PMID: 23519211

Jang-Lee, J., North, S.J., Sutton-Smith, M., Goldberg, D., Panico, M., Morris, H., Haslam, S., Dell, A. Glycomic profiling of cells and tissues by mass spectrometry: fingerprinting and sequencing methodologies. *Meth. Enzymol*. **415,** 59–86 (2006). DOI: 10.1016/S0076-6879(06)15005-3, PMID: 17116468

Johnson, B. A., & Blevins, R. A. NMR View: A computer program for the visualization and analysis of NMR data. *J. Biomol. NMR*. **4**, 603-614 (1994). DOI: 10.1007/BF00404272, PMID: 22911360

Kanagawa, M., Kobayashi, K., Tajiri, M., Manya, H., Kuga, A., Yamaguchi, Y., Manya-Akasaka, K., Furukawa, J.-I., Mizuno, M., Kawakami, H., Shinohara, Y., Wada, Y., Endo,

T., Toda, T. Identification of a Post-translational Modification with Ribitol-Phosphate and Its Defect in Muscular Dystrophy. *Cell Reports* **9**, 2209-2223 (2016). DOI: 10.1016/j.celrep.2016.02.017, PMID: 26923585

Kanagawa, M., Nishimoto, A., Chiyonobu, T., Takeda, S., Miyagoe-Suzuki, Y., Wang, F., Fujikake, N., Taniguchi, M., Lu, Zhongpeng, L., Tachikawa, M., Nagai, Y., Tashiro, F., Miyazaki, J.-I., Tajima, Y., Takeda, S., Endo, T., Kobayashi, K., Campbell, K.P., Toda, T. Residual Laminin-Binding Activity and Enhanced Dystroglycan Glycosylation by LARGE in Novel Model Mice to Dystroglycanopathy. Hum Mol Genet. **18**, 621-631 (2009). DOI: 10.1093/hmg/ddn387, PMID: 19017726

Kanagawa, M., Saito, F., Kunz, S., Yoshida-Moriguchi, T., Barresi, T., Kobayashi, Y.M., Muschler, J., Dumanski, J.P., Michele, D.E., Oldstone, M.B.A., Campbell, K.P. Molecular recognition by LARGE is essential for expression of functional dystroglycan. *Cell*. **117**, 953-964 (2004). DOI: 10.1016/j.cell.2004.06.003, PMID: 15210115

Keller, C., Hansen, M. S., Coffin, C. M., & Capecchi, M. R. Pax3:Fkhr interferes with embryonic Pax3 and Pax7 function: implications for alveolar rhabdomyosarcoma cell of origin. *Genes Dev.* **18**, 2608-2013 (2004). DOI: 10.1101/gad.1243904, PMID: 15520281

Kunz, S., Sevilla, N., McGavern, D. B., Campbell, K. P., & Oldstone, M. B. Molecular analysis of the interaction of LCMV with its cellular receptor α-dystroglycan. *J Cell Biol*. **155**, 301-310 (2001). DOI: 10.1083/jcb.200104103, PMID: 11604425

Mayer, M., & Meyer, B. Group epitope mapping by saturation transfer difference NMR to identify segments of a ligand in direct contact with a protein receptor. *J. Am. Chem. Soc.* **123**, 6108-6117 (2001). DOI: 10.1021/ja0100120, PMID: 11414845

Michele, D. E., Barresi, R., Kanagawa, M., Saito, F., Cohn, R.D., Satz, J.S., Dollar, J., Nishino, I., Kelley, R.I., Somer, H., Straub, V., Mathews, K.D., Moore, S.A., Campbell, K.P. Post-translational disruption of dystroglycan-ligand interactions in congenital muscular dystrophies. *Nature*. **418**, 417-422 (2002). DOI: 10.1038/nature00837, PMID: 12140558

Moracci, M., Ponzano, B.C., Trincone, A., Fusco, S., De Rosa, M., van Der Oost, J., Swensen, C.W., Charlebois, R.L., Rossi, M. Identification and molecular characterization of the first α-xylosidase from an archaeon. *J. Biol. Chem.* **275**, 22082-22089 (2000). DOI: 10.1074/jbc.M910392199, PMID: 10801892

Ohtsubo, K., & Marth, J. D. Glycosylation in cellular mechanisms of health and disease. *Cell*. **126**, 855-867 (2006). DOI: 10.1016/j.cell.2006.08.019, PMID: 16959566

Pinkert, C. A. Ed., *Transgenic Animal Technology: A Laboratory Handbook* (Academic Press, ed. 2, 2002), pp. 20-31.

Rader, E.P, Turk R., Willer T., Beltran D., Inamori K., Peterson, .T.A, Engle, J., Prouty S., Matsumura, K., Saito, F., Anderson M.E., Campbell, K.P. Role of dystroglycan in limiting contraction-induced injury to the sarcomeric cytoskeleton of mature skeletal muscle. *Proc. Natl. Acad. Sci. U.S.A.* **113**, 10992–10997 (2016). DOI: 10.1073/pnas.1605265113, PMID: 27625424

Riemersma, M., Froese, S.D., van Tol, W., Engelke, U.F., Kopec, J., van Scherpenzeel, M., Ashikov, A., Krojer, T., von Delft, F., Tessari, M., Buczkowska, A., Swiezewska, E., Jae, L.T., Brummelkamp, T.R., Manya, H., Endo, T., van Bokhoven, H., Yue, W.W., Lefeber, D.J. Human ISPD Is a Cytidyltransferase Required for Dystroglycan O-Mannosylation. *Chem Biol.* **12**, 1643-1652 (2015). DOI: 10.1016/j.chembiol.2015.10.014, PMID: 26687144

Rowe, R.G. & Weiss, S.J. Breaching the basement membrane: who, when and how? *Trends Cell Biol*. **18**, 560-74 (2008). DOI: 10.1016/j.tcb.2008.08.007, PMID: 18848450

Salleh, H. M., Mullegger, J., Reid, S.P., Chan, W.Y., Hwang, J., Warren, R.A.J., Withers, S.G. Cloning and characterization of Thermotoga maritima β-glucuronidase. *Carbohydr. Res.* **341**, 49-59 (2006). DOI: 10.1016/j.carres.2005.10.005, PMID: 16303119

von Renesse, A., Petkova, M.V., Lutzkendorf, S., Heinemeyer, J., Gill, E., Hübner, C., Moers, A.V., Stenzel, W., Schuelke, M. POMK mutation in a family with congenital muscular dystrophy with merosin deficiency, hypomyelination, mild hearing deficit and intellectual disability. *J Med Genet*. **51**, 275-282 (2014). DOI: 10.1136/jmedgenet-2013-102236, PMID: 24556084

Willer, T., Inamori, K., Venzke, D., Harvey, C., Morgensen, G., Hara, Y., Beltran Valero de Bernabe, D., Yu, L.., Wright, K.M., Campbell, K.P. The glucuronyltransferase B4GAT1 is required for initiation of LARGE-mediated α-dystroglycan functional glycosylation. *eLife*. **3**, e03941 (2014). DOI: 10.7554/eLife.03941, PMID: 25279699

Willer, T., Lee, H., Lommel, M., Yoshida-Moriguchi, T., Beltran Valero de Bernabe, D., Venzke, D., Cirak, S., Schachter, H., Vajsar, J., Voit, T., Muntoni, F., Loder, A.S., Dobyns, W.B., Winder, T.L., Strahl, S., Mathews, K.D., Nelson, S.F., Moore, S.A., Campbell, K.P. ISPD loss-of-function mutations disrupt dystroglycan O-mannosylation and cause Walker-Warburg syndrome. *Nat Genet*. **44**, 575-580 (2012). DOI: 10.1038/ng.2252, PMID: 22522420

Yoshida-Moriguchi, T. & Campbell, K. P. Matriglycan: a novel polysaccharide that links dystroglycan to the basement membrane. *Glycobiology.* **25,** 702-713 (2015). DOI: 10.1093/glycob/cwv021, PMID: 25882296

Yoshida-Moriguchi, T., Willer, T., Anderson, M.E., Venzke, D., Whyte, T., Muntoni, F., Lee, H., Nelson, S.F., Yu, L., Campbell, K.P. SGK196 is a glycosylation-specific *O*-mannose kinase required for dystroglycan function. *Science*. **341,** 896-899 (2013). DOI: 10.1126/science.1239951, PMID: 23929950

Yoshida-Moriguchi, T., Yu, L., Stalnaker, S.H., Davis, S., Kunz, S., Madson, M., Oldstone, M.B.A., Schachter, H., Wells, L., Cambell, K.P. *O*-mannosyl phosphorylation of α-dystroglycan is required for laminin binding. *Science.* **327**, 88-92 (2010). DOI: 10.1126/science.1180512, PMID: 20044576

Zhang, H., Zhu, F., Yang, T., Ding, L., Zhou, M., Li, J., Haslam, S.M., Dell, A., Erlandsen, H., Wu, H. The highly conserved domain of unknown function 1792 has a distinct glycosyltransferase fold. *Nat Commun.* **5,** 4339 (2014). DOI: 10.1038/ncomms5339, PMID: 25023666

Zhu, Q., Venzke, D., Walimbe, A.S., Anderson, M.E., Fu, Q., Kinch, L.N., Wang, W., Chen, X., Grishin, N.V., Huang, N., Yu, L., Dixon, J.E., Campbell, K.P., Xiao, J. Structure of protein *O*-mannose kinase reveals a unique active site architecture. *eLife*. **5**, e22238 (2016). DOI: 10.7554/eLife.22238, PMID: 27879205

SUPPLEMENTARY TEXT

We transduced *POMK/DG* KO HAP1 and *POMK* KO HAP1 cells with an adenovirus expressing wild-type DG (Ad-DG). We observed a return of the laminin binding at 90-100 kDa in *POMK/DG* KO HAP1 cells (***Figure 7-Figure Supplement 4A***) and an increase in the corresponding IIH6 immunoreactivity and laminin binding in *POMK* KO HAP1 cells (***Figure 7-Figure Supplement 6A, 6B, 6C***), further indicating that the glycoprotein responsible is α-DG.

The binding of a xylose-glucuronic acid repeat of matriglycan to the LG-domains of ECM ligands is calcium-dependent **(*Yoshida-Moriguchi et al., 2015; Hohenester, 2019; Briggs et al., 2016*)**. To test if the binding of the non-extended matriglycan is similarly calcium-dependent, we performed laminin overlays in the presence of 10 mM EDTA (***Figure 7-Figure Supplement 6D, 6E***). In both WT and *POMK* KO HAP1 cells, there was a complete absence of laminin binding in the presence of EDTA, indicating that laminin binding at 90-100 kDa is calcium-dependent and the glycan responsible is composed of xylose-glucuronic acid repeats.

Given the higher affinity of POMK for the unphosphorylated core M3 compared to the phosphorylated form (***Figure 8C; Figure 8-Figure Supplement 1A***), it is possible that POMK D204N, which is catalytically inactive, binds to GGM and increases the amount of core M3-modifed α-DG in the ER, thereby reducing the amount entering the Golgi. With a reduction in the amount of core M3-modified α-DG entering the Golgi, FKTN may be able to better modify GalNac of the unphosphorylated core M3, thus enabling the formation of the matriglycan which enables laminin binding at 90-100 kDa in the patient's skeletal muscle. In *POMK* KO HAP1 cells alone, the non-extended matriglycan represents the amount formed when no POMK is present and transport of core M3-modified α-DG to the Golgi is not reduced. In support of this hypothesis, overexpression of POMK D204N in *POMK* KO HAP1 cells at a higher multiplicity of infection (MOI) of 10 leads to higher MW forms of matriglycan despite the catalytic inactivity of POMK D204N *in vitro* (***Figure 7-Figure Supplement 6F***). The higher MW of this form of matriglycan resembles that of the POMK D204N skeletal muscle. Alternatively, it is possible that POMK D204N remains attached to the unphosphorylated core M3 and this binary complex of POMK D204N and α-DG moves to the Golgi, where it can form a ternary complex with FKTN. The ternary complex composed of FKTN, POMK D204N, and α-DG enables FKTN to more efficiently elongate the core M3 leading to formation of the non-extended matriglycan. Further studies will be needed to determine the precise mechanism.

Supplementary Figures

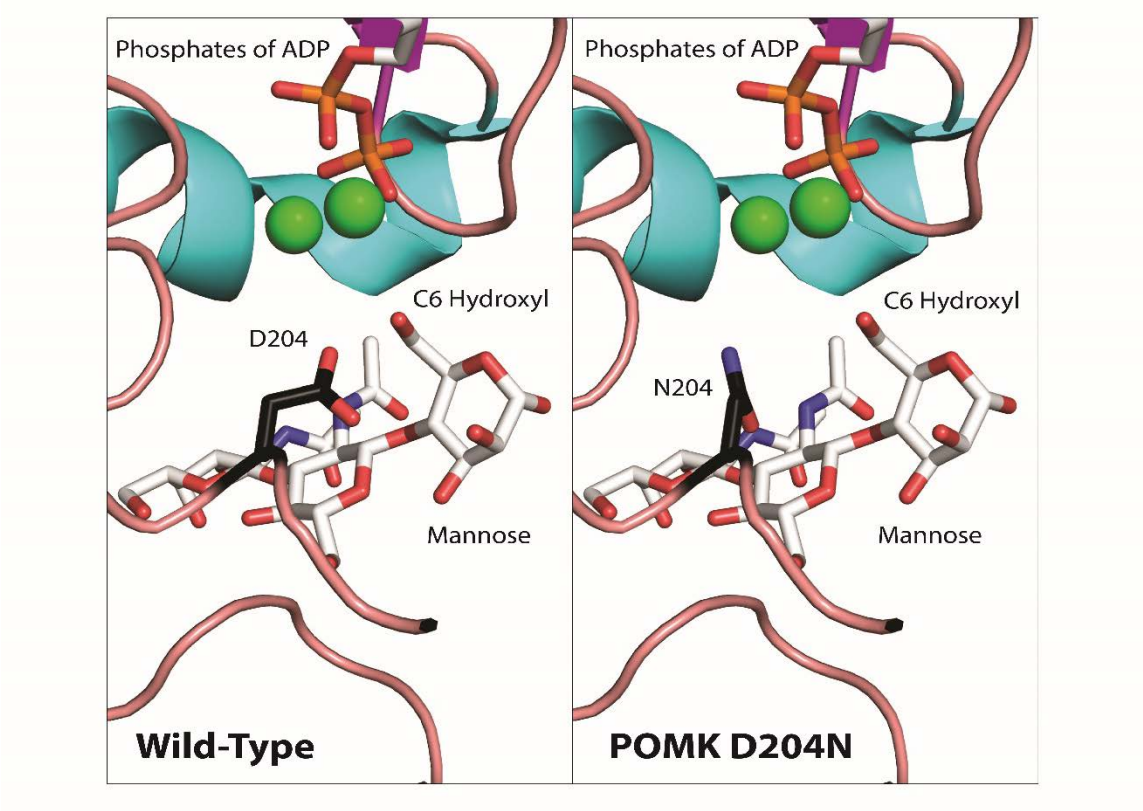

Figure 2 - Figure Supplement 1. Structural Modeling of POMK D204N Mutation. This figure shows structural modeling of wild-type POMK and the POMK D204N mutation using human POMK protein sequence numbering, based on the crystal structure of Zebrafish POMK. The green spheres indicate manganese ions. The phosphorous, oxygen, nitrogen, and carbon atoms are colored in orange, red, blue, and white, respectively. The D204 and N204 carbon atoms are colored dark. The gamma phosphate of ATP is not shown.

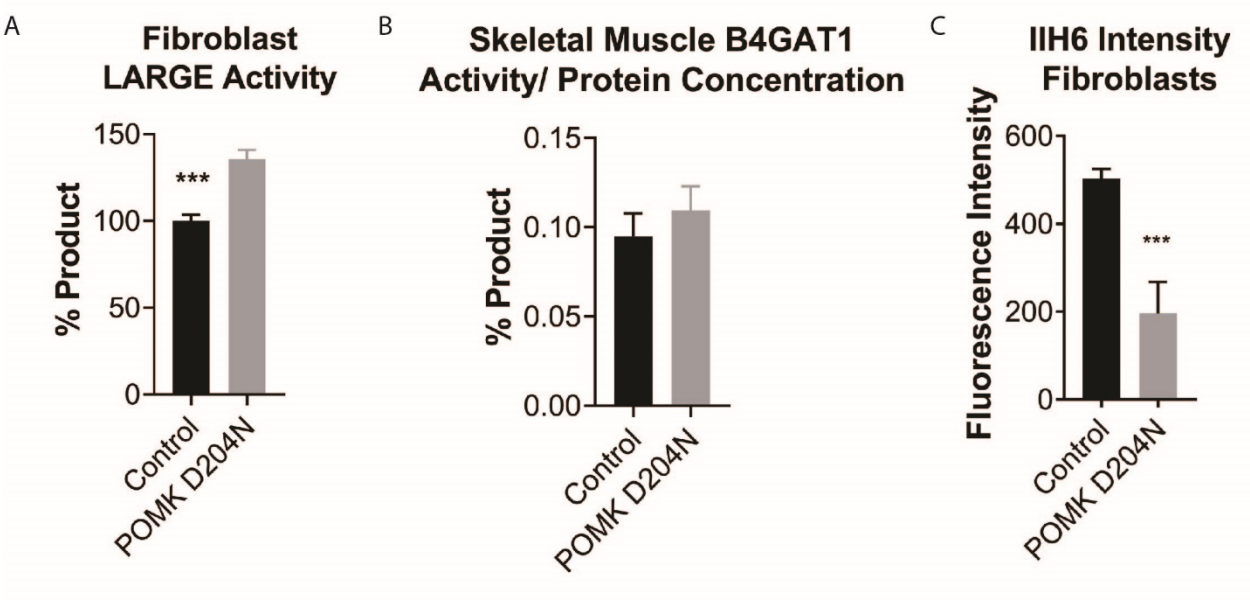

Figure 2 - Figure Supplement 2. Supplemental Analysis of POMK D204N Fibroblasts and Muscle. **A,** LARGE activity in control human fibroblasts and fibroblasts from patient NH13-284 (POMK D204N). Triple asterisks indicate p-value<0.001 using Student's unpaired t-test (three replicates). **B,** B4GAT1 activity (normalized to protein concentration) from control human skeletal muscle and POMK D204N muscle. **C,** Mean fluorescence intensity of control human fibroblasts and POMK D204N fibroblasts. Flow cytometry analyses were performed using an antibody against matriglycan (IIH6). Triple asterisks indicate statistical significance with p-value<0.001 using Student's unpaired t-test (three replicates).

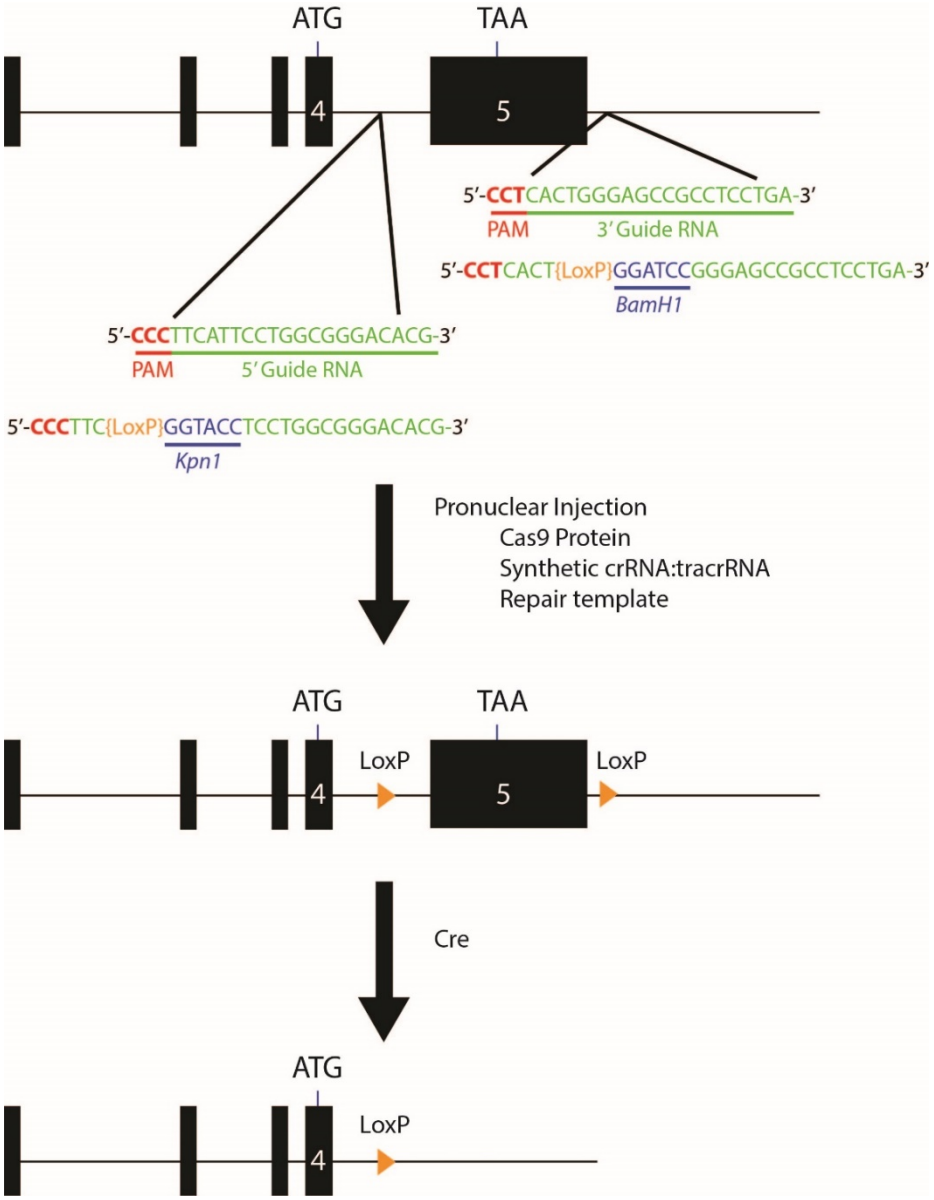

Figure 3 - Figure Supplement 1. Schematic for Generation of Floxed Alleles of *POMK*. Map of 5' and 3' LoxP sites (orange). LoxP sites flanking exon 5 of *POMK* (large black box), which encodes the majority of the kinase domain of POMK, were inserted using CRISPR/Cas9. Cre-mediated recombination of the floxed allele of *POMK* is predicted to lead to a loss of exon 5.

A B

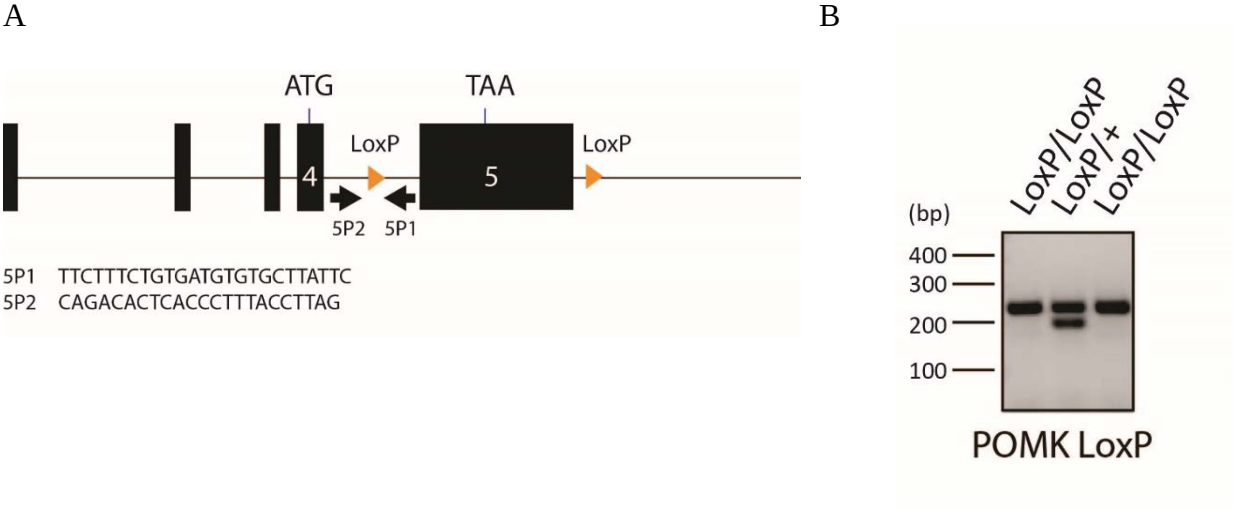

Figure 3 - Figure Supplement 2. Results of *POMK*^{LoxP} Genotyping. **A,** Genotyping Strategy for floxed *POMK* Allele. PCR Primers were designed to flank the 5' LoxP site. **B,** the *wild-type* allele is 197 bp, while the *LoxP* allele is 235 base pairs.

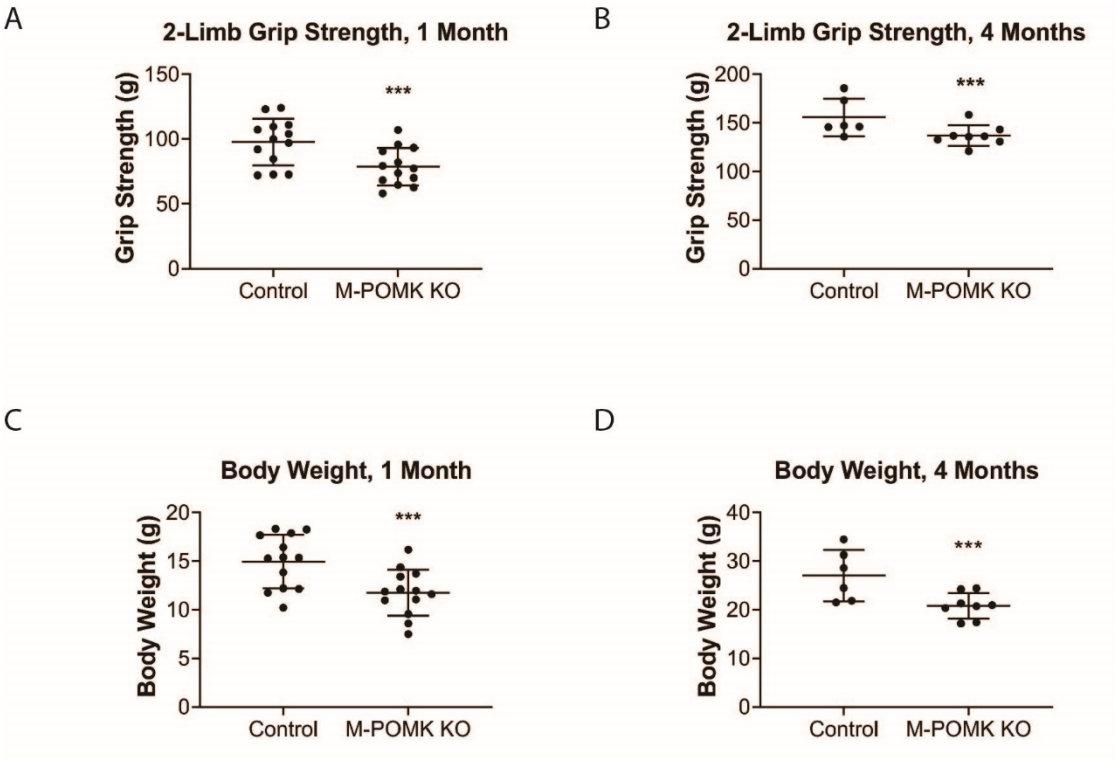

Figure 3 - Figure Supplement 3. Muscle-Specific POMK Knockout Mice Have Reduced Grip Strength and Body Weight. **A, B,** 2-limb grip strength of 1-month old (**A**) and 4-month old (**B**) $POMK^{LoxP/LoxP}$ (Control) and MCK-Cre; Pax7-Cre; $POMK^{LoxP/LoxP}$ (M-POMK KO) mice. **C, D,** Body weights of 1-month old (**C**) and 4-month old (**D**) Control and M-POMK KO mice. Triple asterisks: p-value < 0.05 using Student's unpaired t-test.

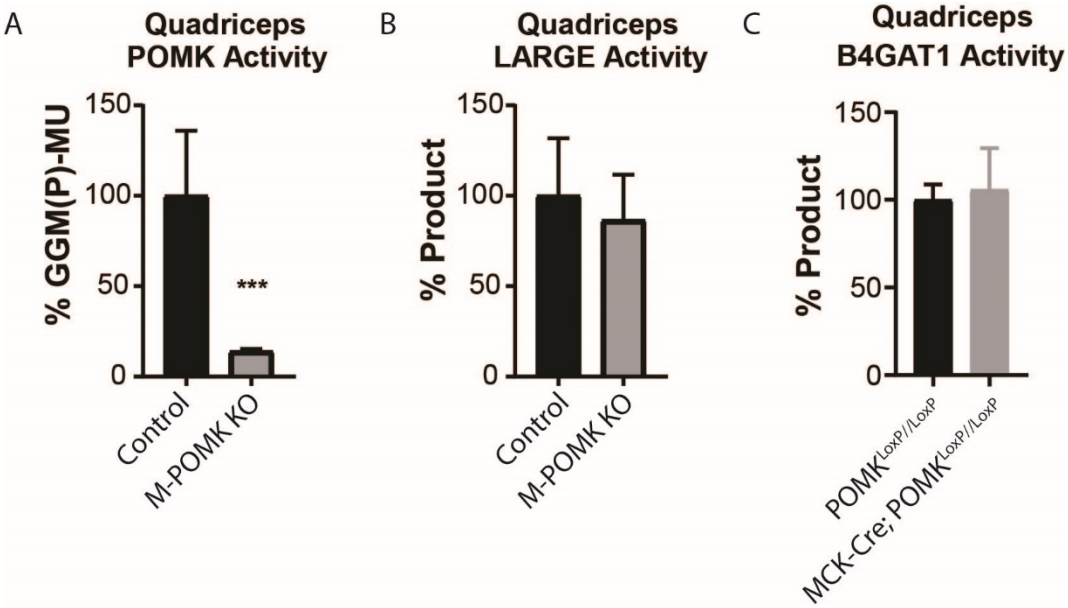

Figure 3 - Figure Supplement 4. Supplemental Biochemical Analysis of POMK Null Skeletal Muscle. **A, B,** POMK (**A**) and LARGE (**B**) activity of M-POMK KO and $POMK^{LoxP/LoxP}$ (Control) quadriceps muscle extracts (three replicates). Asterisks indicate P-value=0.01 using Student's unpaired t-test. **C,** B4GAT1 activity in MCK-Cre; $POMK^{LoxP/LoxP}$ and control quadriceps muscle extracts (three replicates).

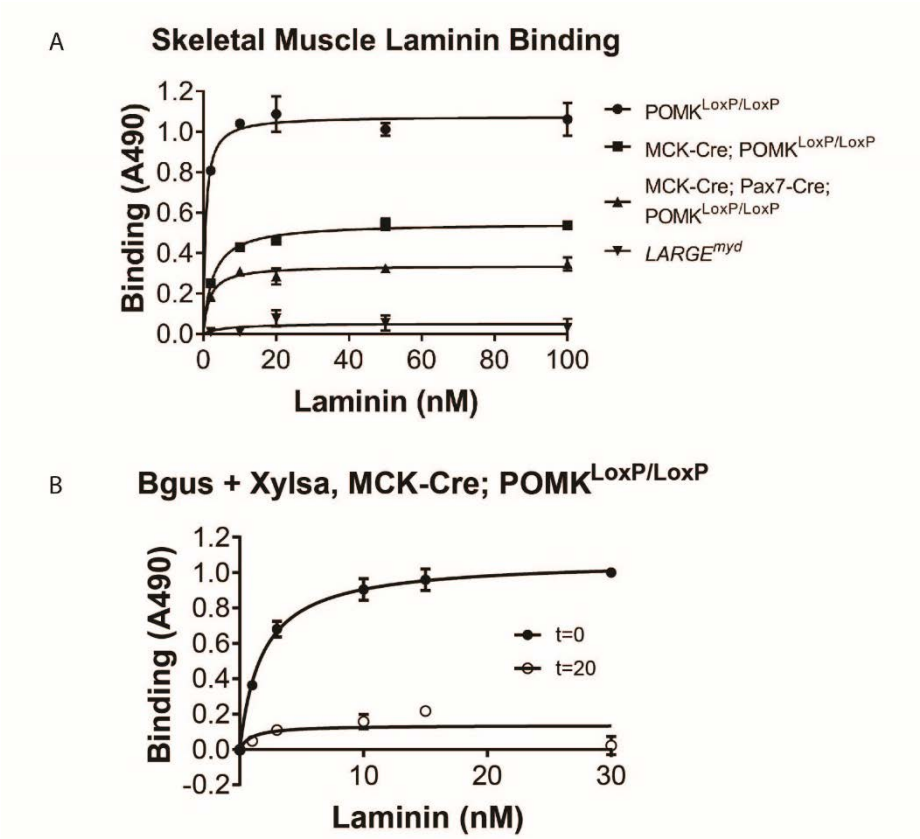

Figure 5 - Figure Supplement 1. Solid-Phase Binding Analyses of POMK KO Skeletal Muscle. **A,** Solid-phase binding analysis (relative B_{max} for laminin-111) of control, M-POMK KO (MCK-Cre; Pax7-Cre; POMK$^{LoxP/LoxP}$), MCK-Cre; POMK$^{LoxP/LoxP}$, and *LARGE^{myd}* skeletal muscle (three replicates). Error bars: standard deviation. **B,** Solid-phase binding analysis of MCK-Cre; POMK$^{LoxP/LoxP}$ skeletal muscle treated in combination with Xylsa and Bgus for 0 or 20 hours. Results from three independent experiments are shown. Error bars: standard deviation.

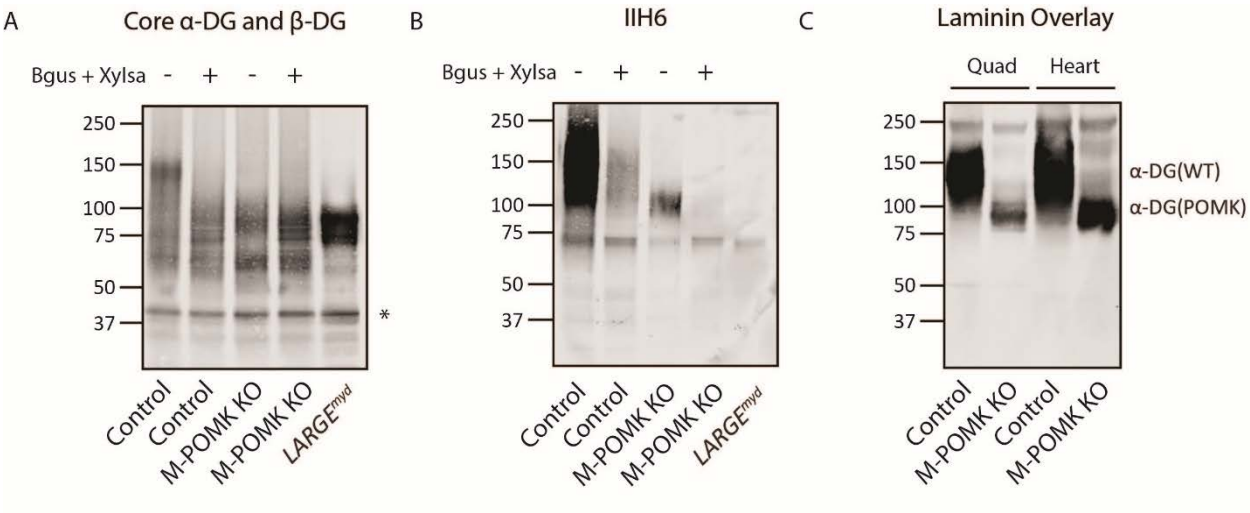

Figure 5 - Figure Supplement 2. POMK Knockout Muscle Expresses Matriglycan. **A, B,** Glycoproteins were enriched from skeletal muscles of M-POMK KO, control, and *LARGE*^{myd} mice and treated in combination with α-xylosidase (Xylsa) and β-glucuronidase (Bgus). Immunoblotting was performed with **A**, AF6868 (core α-DG and β-DG) and **B**, IIH6 (matriglycan). Results from three independent experiments are shown. Asterisk: β-DG. **C**, A laminin overlay was performed of control M-POMK KO skeletal muscle and heart. Glycoproteins were enriched from heart as above (three replicates).

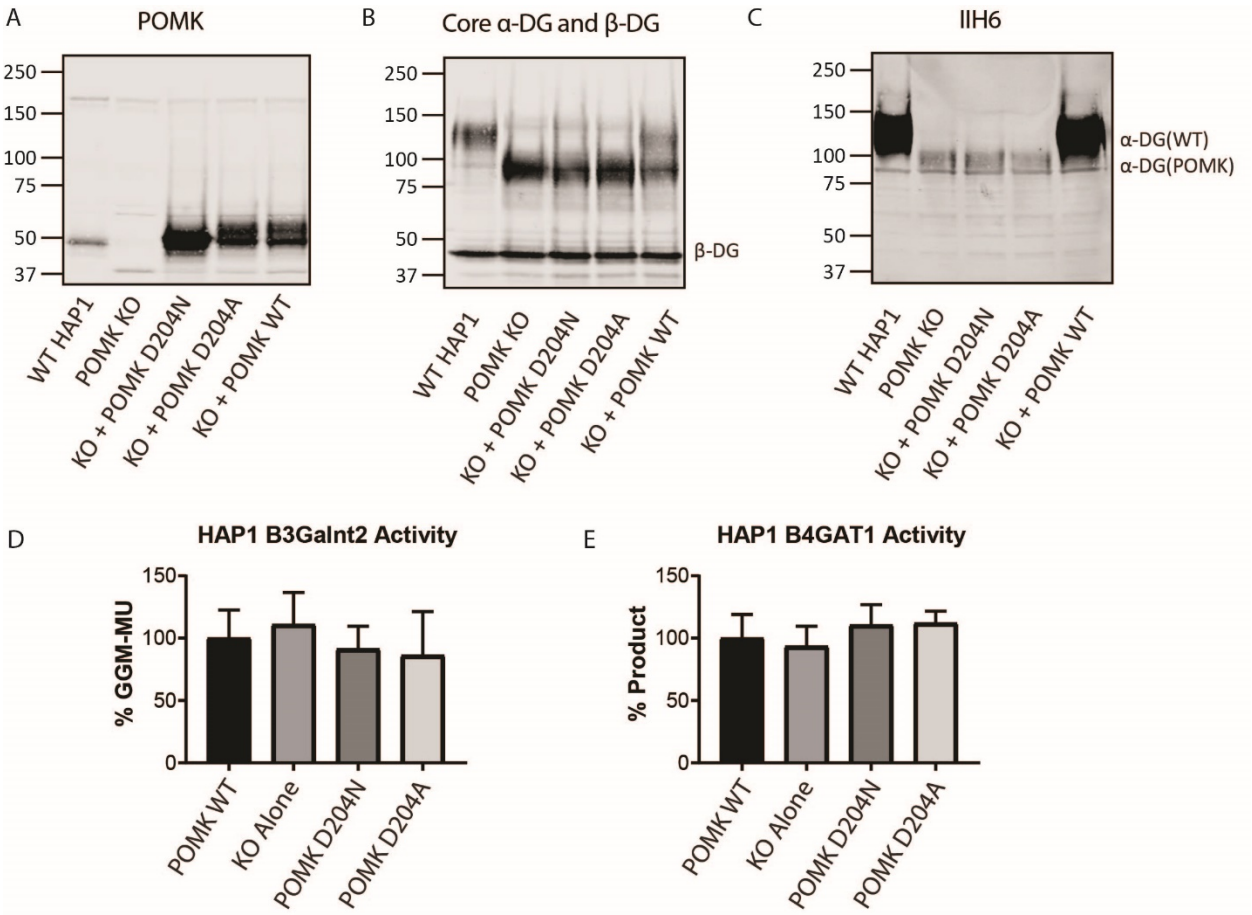

Figure 6 - Figure Supplement 1. Supplemental Biochemical Analysis of POMK D204N and *POMK* KO HAP1 Cells. **A, B, C:** *POMK* KO HAP1 cells were transduced with the indicated adenoviruses and immunoblotting was performed for: **A,** POMK, **B,** Core α-DG and β-DG, and **C**, matriglycan (IIH6), (three replicates). **D,** B3GALNT2 and E, B4GAT1 activity of *POMK* KO HAP1 cells expressing POMK mutants. Activity of each mutant relative to WT POMK is depicted. (Error bars: standard deviation). Results from three independent experiments are shown.

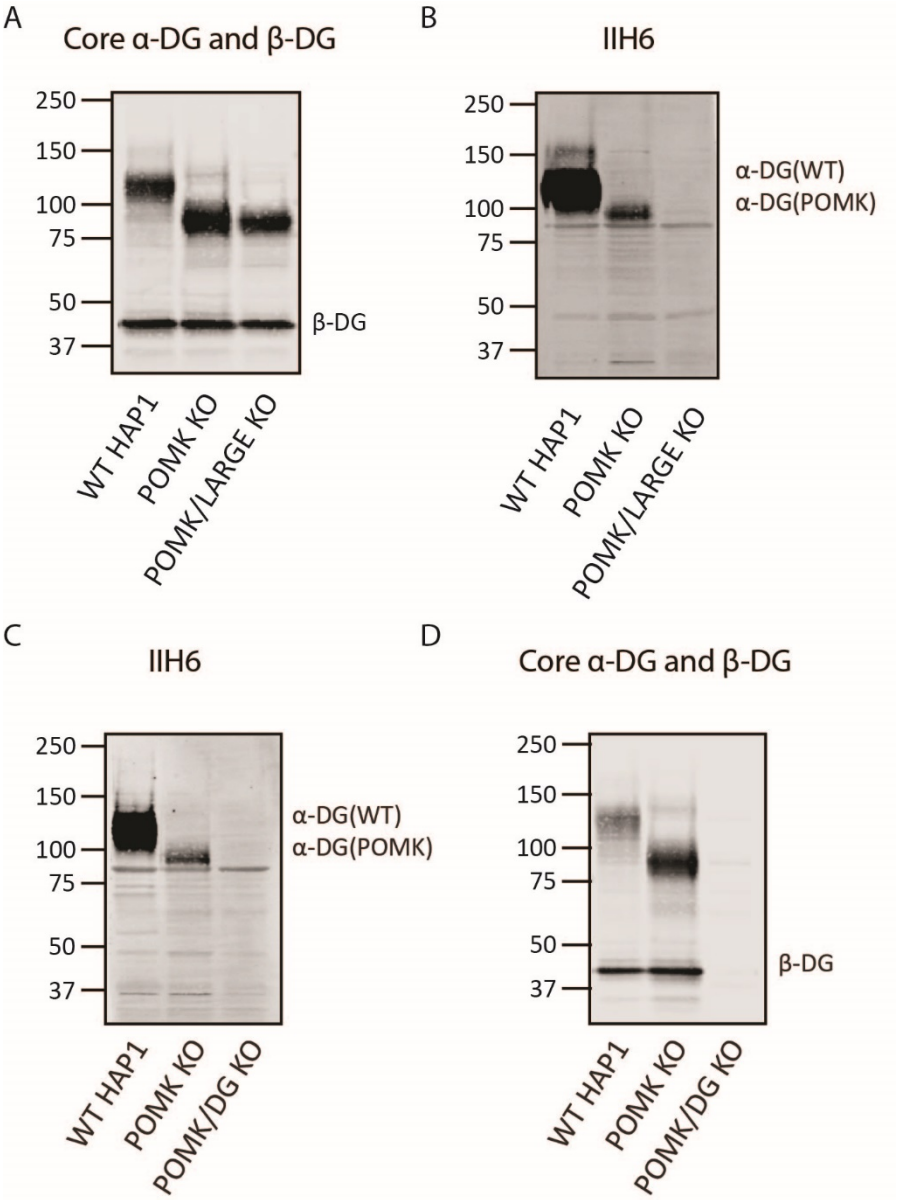

Figure 7 - Figure Supplement 1. Supplemental Biochemical Analysis of *POMK/LARGE* KO and *POMK/DG* KO HAP1 Cells. **A, B** Immunoblotting of WT, *POMK* KO and *POMK/LARGE* KO HAP1 cells with antibodies AF6868 (**A),** Core α-DG and β-DG) or IIH6 (**B**). Glycoproteins were enriched using WGA-agarose as described in the Methods. **C, D** Immunoblotting of WT, *POMK* KO, and *POMK/DG* KO HAP1 cells with antibodies IIH6 (**C**) or AF6868 (**D**, Core α-DG and β-DG). Representative results from three independent experiments are shown.

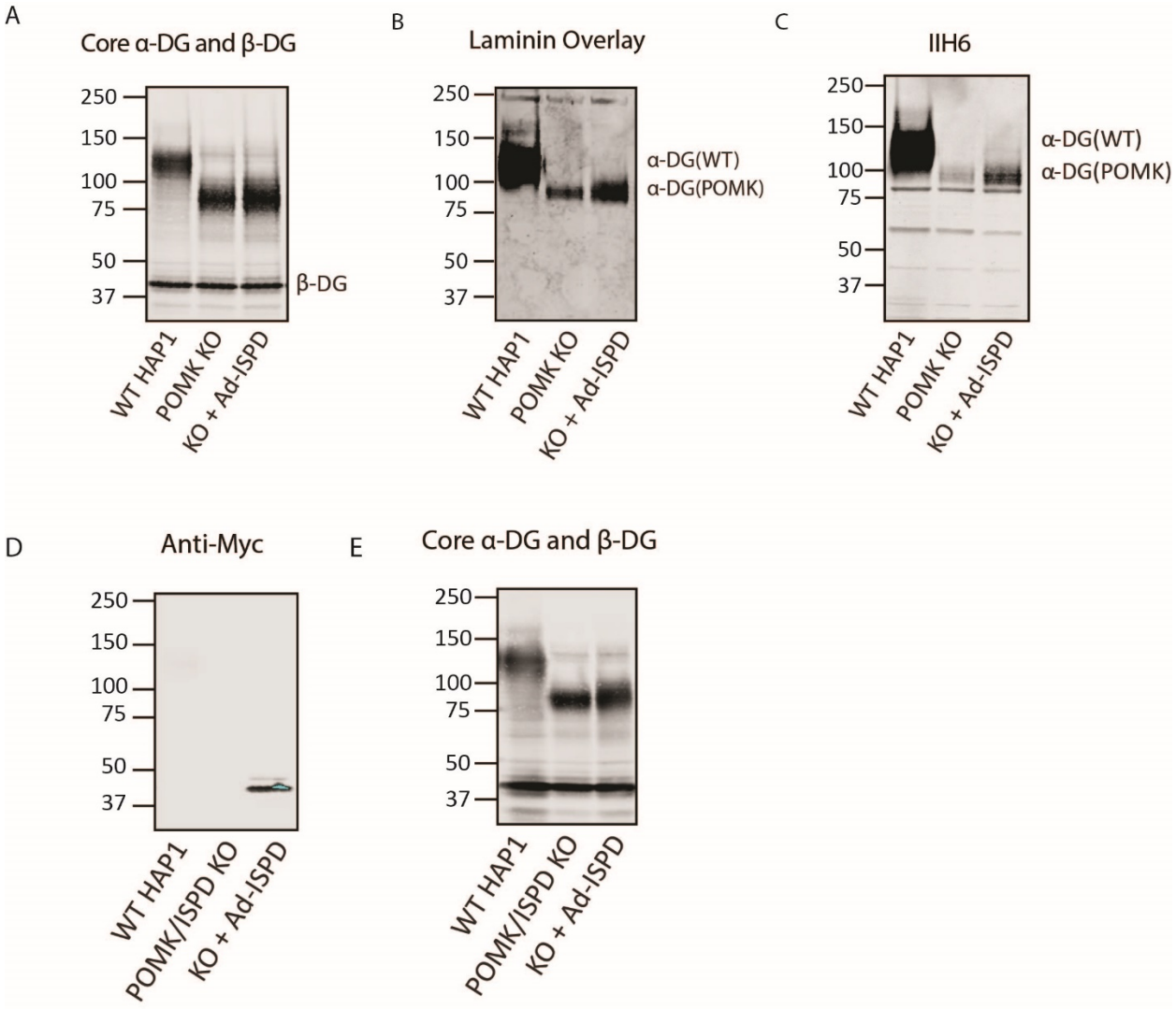

Figure 7 - Figure Supplement 2. Requirement for Ribitol-Phosphate in the Synthesis of the Non-Extended Matriglycan. **A, B, C**, *POMK* KO HAP1 cells were transduced with an adenovirus encoding Isoprenoid Synthase Domain-Containing (Ad-*ISPD*). Immunoblotting was performed using antibodies AF6868 (**A**) or IIH6 (**C**). **B**, A laminin overlay was also performed. Representative results from three independent experiments are shown. **D**, **E,** HAP1 cells lacking expression of ISPD and POMK (*POMK/ISPD* KO) were transduced with Ad-*ISPD*. Immunoblotting was performed with an anti-Myc antibody (**D**) or antibody AF6868 (**E**, Core α-DG and β-DG). Representative results from three independent experiments are shown.

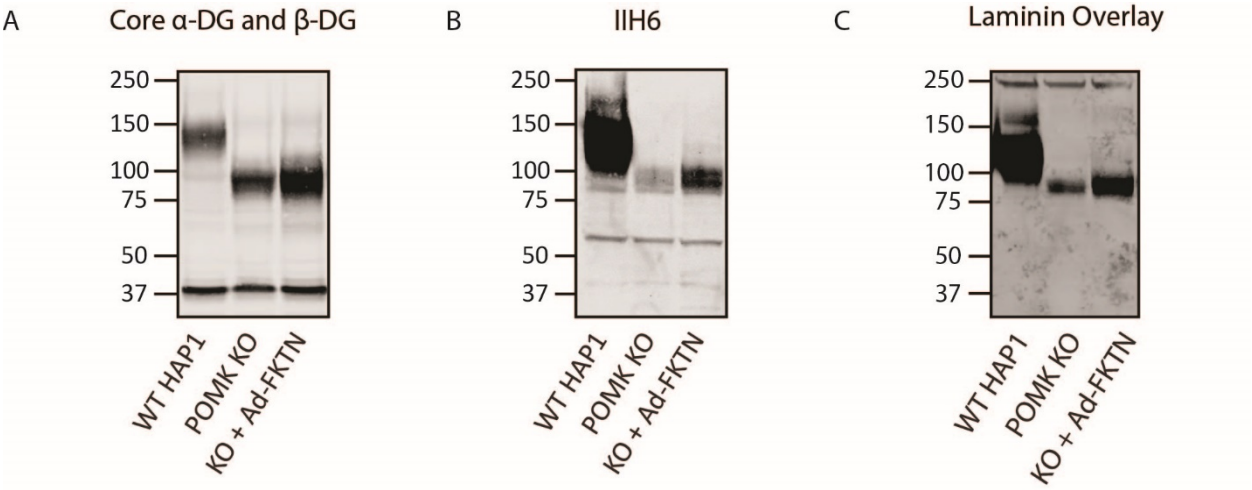

Figure 7 - Figure Supplement 3. Fukutin Overexpression Enhances Synthesis of the Non-Extended Matriglycan. **A, B, C**, *POMK* KO HAP1 cells transduced with an adenovirus encoding Fukutin (FKTN), Ad-*FKTN*. Immunoblotting was performed using antibodies AF6868 (**A)**, Core α-DG and β-DG) or IIH6 (**B)** (three replicates). **C**, A laminin overlay was also performed (three replicates).

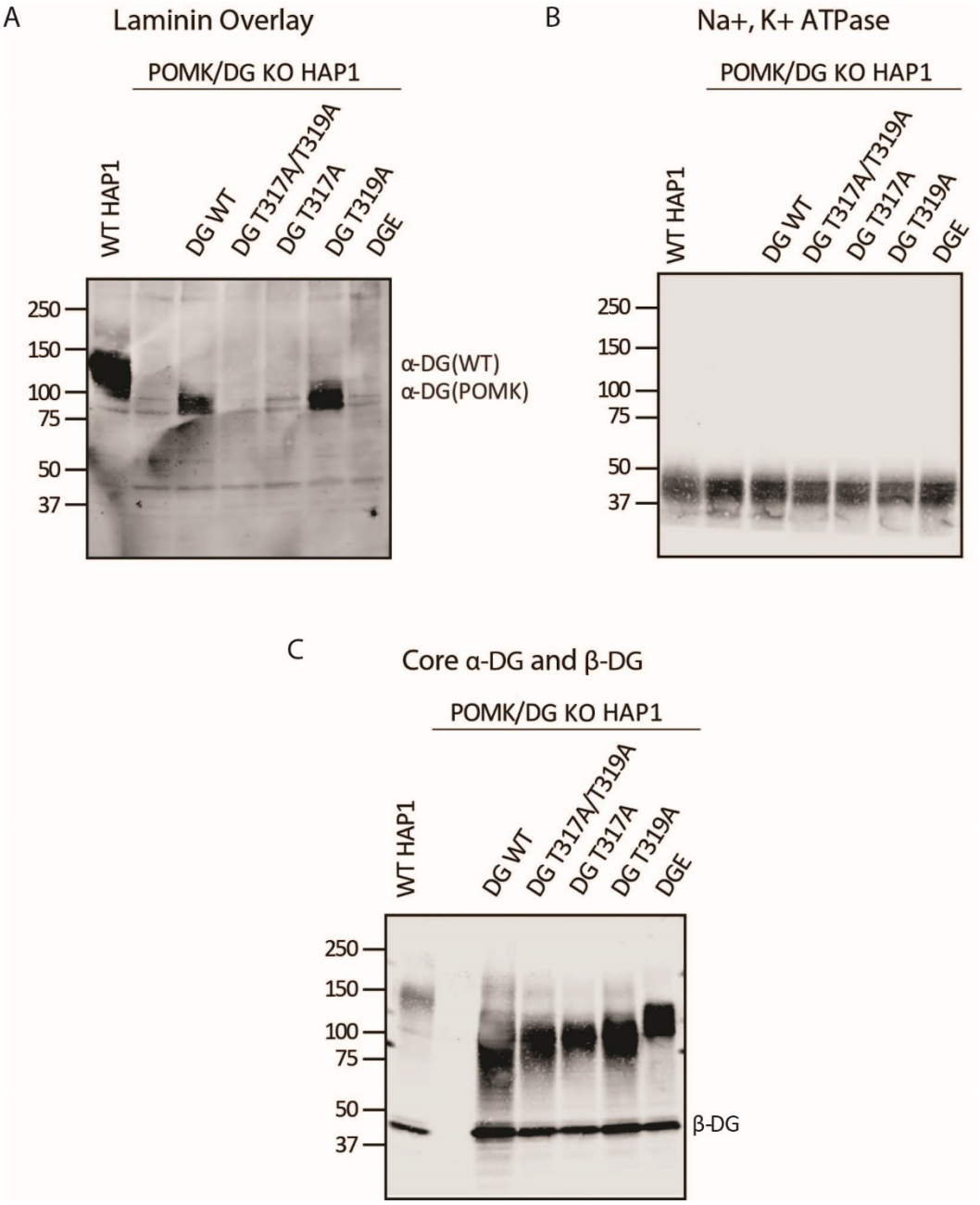

Figure 7 - Figure Supplement 4. T317 is Required for Synthesis of the Non-Extended Matriglycan. **A, B, C** Biochemical analysis of *POMK/DG* KO HAP1 cells expressing the indicated adenoviruses (three replicates). DGE is for viral expression of α-DG that lacks the Dystroglycan N-terminal domain (DGN). **A**, A laminin overlay was performed. Immunoblotting was performed with an Na+/K+ ATPase antibody (**B**) and antibody AF6868 (**C**, Core α-DG and β-DG).

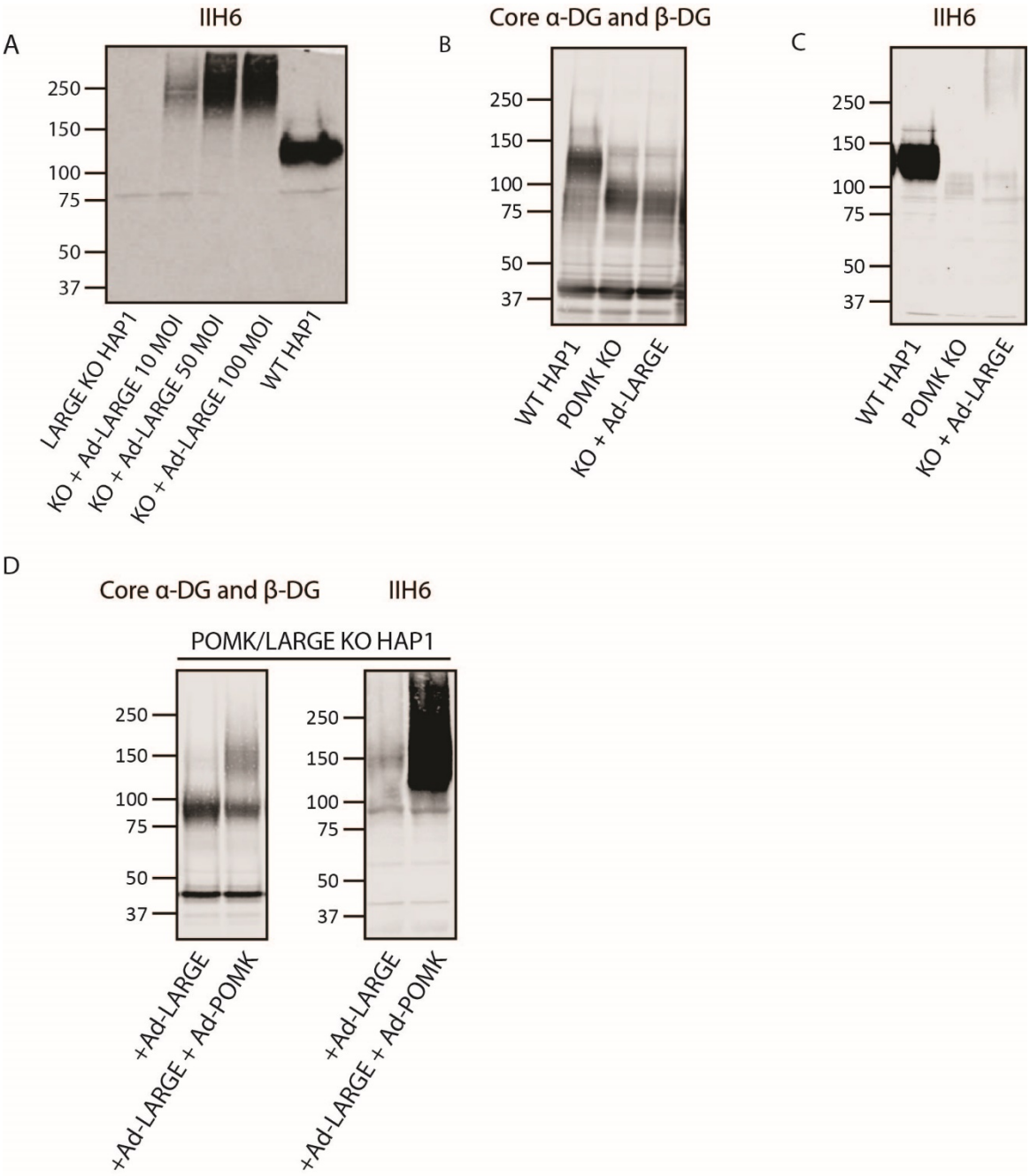

Figure 7 - Figure Supplement 5. POMK Enables LARGE-mediated Elongation of Matriglycan. **A, B, C,** Immunoblots of the following HAP1 cells: **A**, *LARGE* KO, overexpressing Ad-*LARGE*; **B**, **C**, *POMK* KO, overexpressing Ad-*LARGE*; **D,** *POMK/LARGE* KO, overexpressing Ad-*LARGE* with or without Ad-*POMK*. Immunoblotting was performed with antibodies AF6868 (Core α-DG and β-DG) or IIH6 (three replicates).

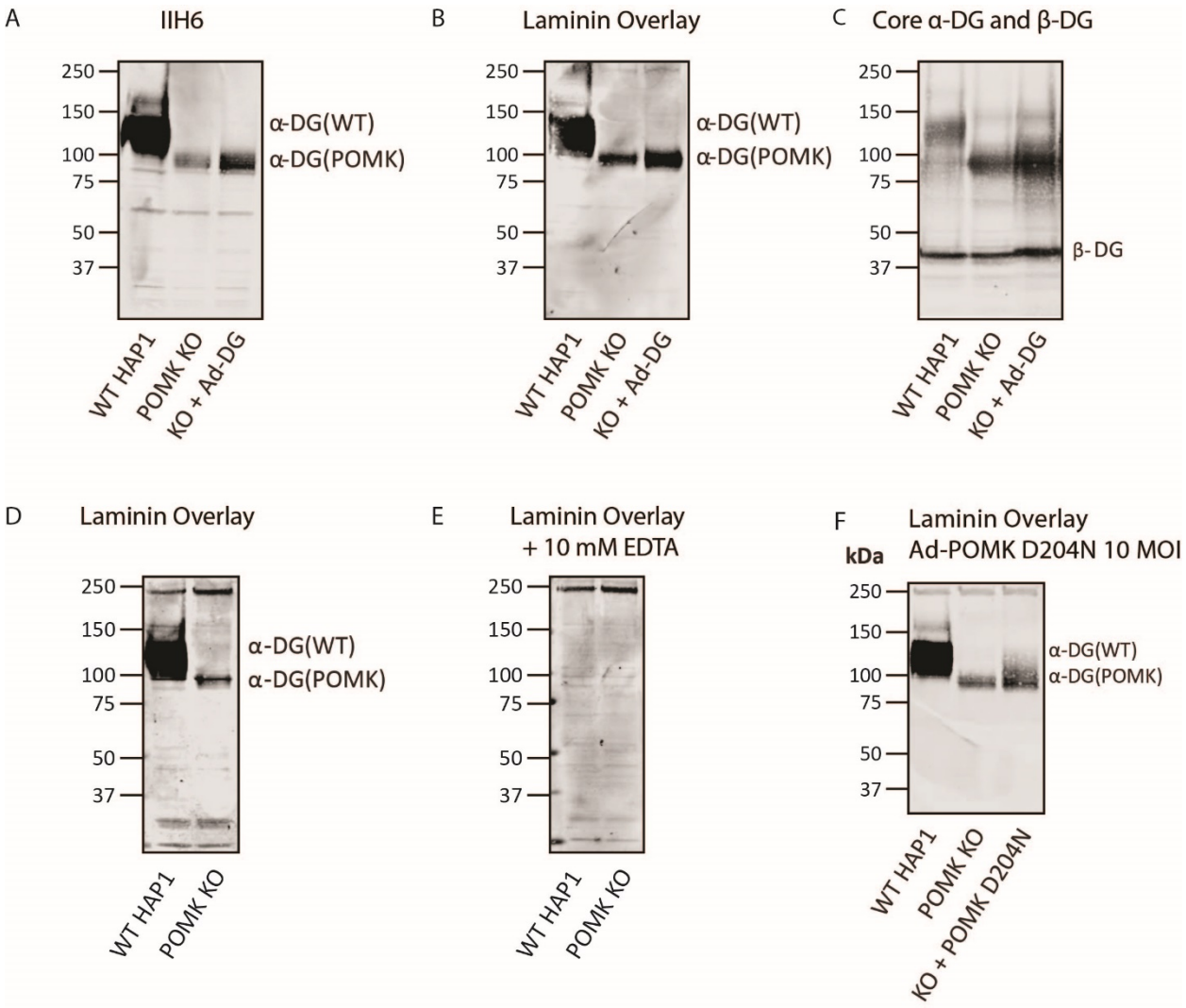

Figure 7 - Figure Supplement 6. Supplemental Characterization of POMK-null Matriglycan Synthesis. **A**, **B**, **C**, *POMK* KO HAP1 cells were transduced with an adenovirus encoding DG (Ad-DG) and immunoblotting was performed with antibodies IIH6 (**A**) and AF6868 (**C**) (three replicates). A laminin overlay was also performed (**B**) (three replicates). **D, E,** Laminin overlays of WT and *POMK* KO HAP1 cells were performed without (**D**) or with (**E**) EDTA (three replicates). **F**, A laminin overlay of WT HAP1, *POMK* KO HAP1, or *POMK* KO HAP1 cells transduced with 10 MOI Ad-*POMK* D204N was performed (three replicates).

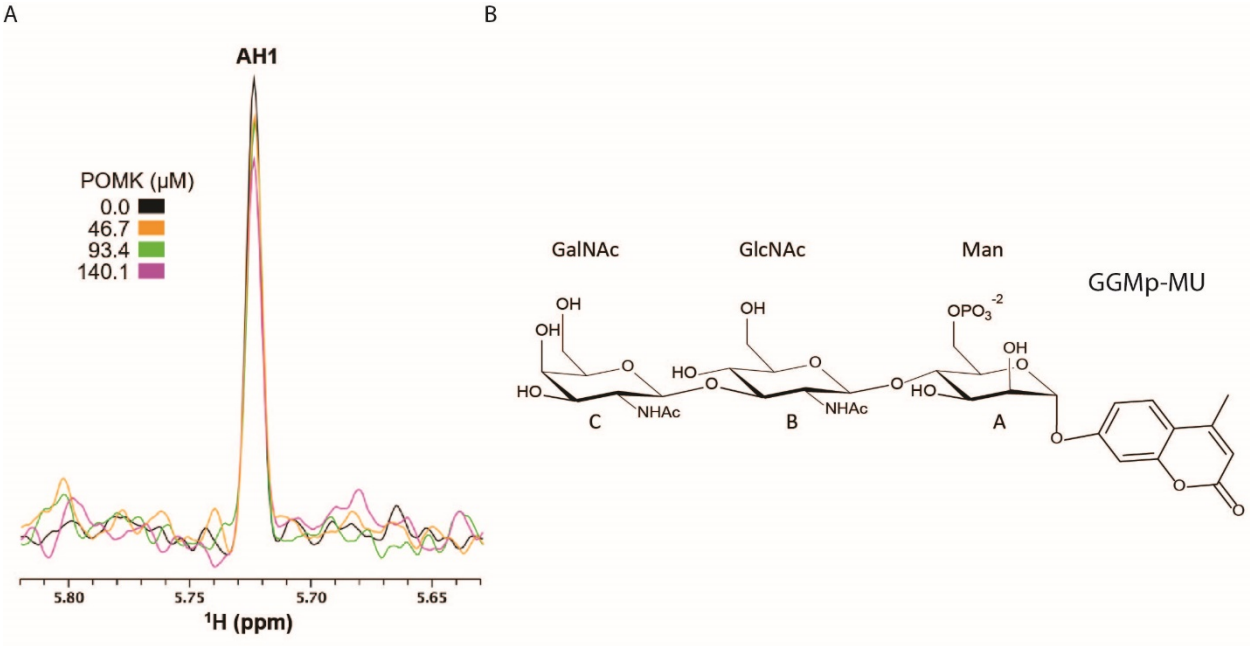

Figure 8 - Figure Supplement 1. NMR Spectra of POMK Binding to GGMp-MU and Structure of GGMp-MU. **A,** 1D ^{1}H NMR spectra of the glycan sample (10.0 µM GGMp-MU) were acquired in the presence of various concentrations of zebrafish POMK as indicated. The ^{13}C and ^{1}H resonances of GGMp-MU have been assigned before **(*Yoshida-Moriguchi et al., 2013*)**. The peak AH1 is derived from the residue A (Man) anomeric H1 proton. **B,** Chemical structure of GGMp-MU.

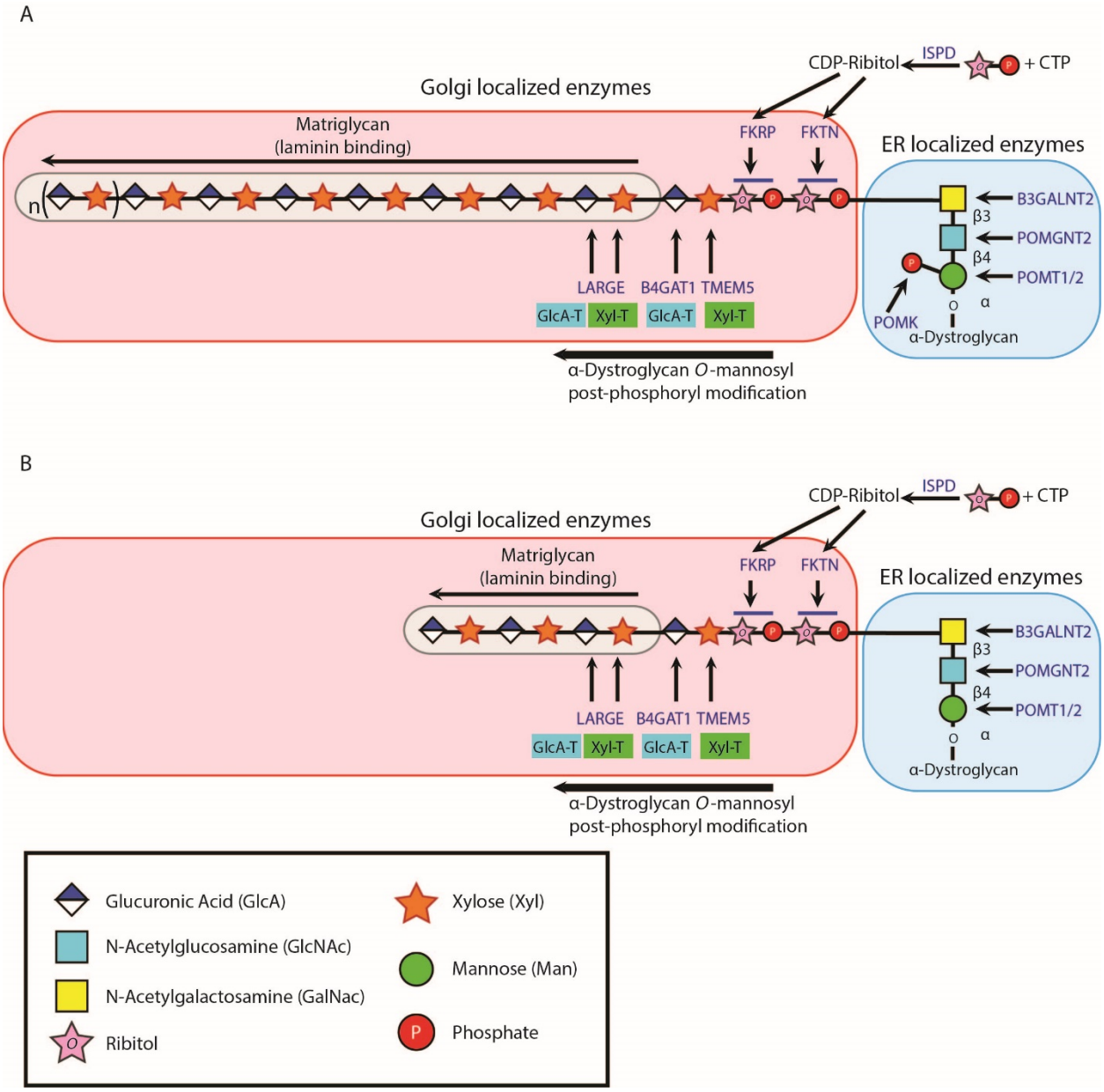

Figure 8 - Figure Supplement 2. Model of Full-Length and Non-extended Matriglycan Synthesis. **A,** Mature matriglycan is a long polysaccharide that is synthesized by LARGE. **B,** In the absence of the core M3 phosphate added by POMK, LARGE generates a shorter, non-extended form of matriglycan.

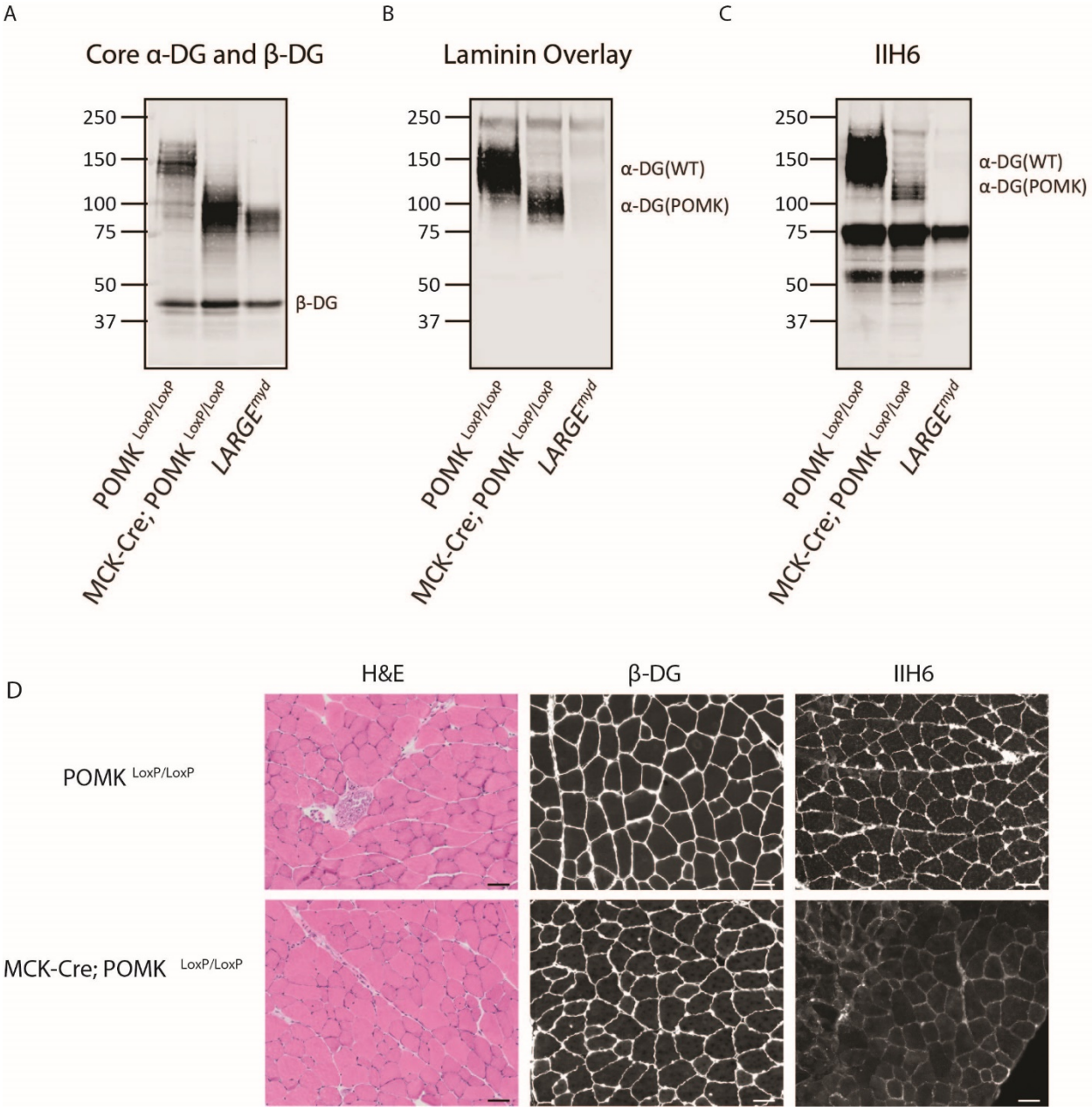

Figure 8 - Figure Supplement 3. Biochemical and Histologic Analysis of MCK-Cre; POMK$^{LoxP/LoxP}$ Quadriceps Muscle. **A, B, C,** Representative biochemical analysis of glycoproteins enriched from quadriceps skeletal muscles of POMK$^{LoxP/LoxP}$, MCK-Cre; POMK$^{LoxP/LoxP}$, and *LARGE^{myd}* mice using WGA-agarose (three replicates). For immunoblotting, antibodies AF6868 (**A**) and IIH6 (**C**) were used, and a laminin overlay was also performed (**B**). **D**, Immunofluorescence and H&E analyses of POMK$^{LoxP/LoxP}$ and MCK-Cre; POMK$^{LoxP/LoxP}$ quadriceps muscle sections from 8-month old mice. Sections were stained with antibodies against β-DG (middle) and matriglycan (IIH6) (right). Histologic abnormalities in the sections were evaluated by means of hematoxylin and eosin (H&E) staining (left). Scale bars- 50 µM (three replicates).